

PAPER • OPEN ACCESS

First observation and interpretation of spontaneous collective radiation from fusion-born ions in a stellarator plasma

To cite this article: B C G Reman *et al* 2022 *Plasma Phys. Control. Fusion* **64** 085008

View the [article online](#) for updates and enhancements.

You may also like

- [On a fusion chain reaction via suprathreshold ions in high-density H-¹¹B plasma](#)
Fabio Belloni
- [Unstable spectra of plane Poiseuille flow with a uniform magnetic field](#)
Lai Wei, Yunxia Liu, Fang Yu et al.
- [Isotope effects of trapped electron modes in the presence of impurities in tokamak plasmas](#)
Yong Shen, J Q Dong, A P Sun et al.









IOP | ebooks™

Bringing together innovative digital publishing with leading authors from the global scientific community.

Start exploring the collection—download the first chapter of every title for free.

First observation and interpretation of spontaneous collective radiation from fusion-born ions in a stellarator plasma

B C G Reman^{1,8,*} , R O Dendy^{1,2}, H Igami³ , T Akiyama^{3,9}, M Salewski⁴,
S C Chapman¹ , J W S Cook^{1,2}, S Inagaki^{5,10} , K Saito³, R Seki³, M Toida³, M H Kim⁶ ,
S G Thatipamula⁷ and G S Yun⁷ 

¹ Centre for Fusion, Space and Astrophysics, Department of Physics, Warwick University, Coventry CV4 7AL, United Kingdom

² CCFE, Culham Science Centre, Abingdon, Oxfordshire OX14 3DB, United Kingdom

³ National Institute for Fusion Science, Toki, Gifu 509-5292, Japan

⁴ Department of Physics, Technical University of Denmark, Fysikvej, Building 309, 2800 Kongens Lyngby, Denmark

⁵ Research Institute for Applied Mechanics, Kyushu University, Kasuga, Fukuoka 816-8580, Japan

⁶ Korea Institute of Fusion Energy, 169-148 Gwahak-ro, Daejeon, Yuseong-gu, 34133, Republic of Korea

⁷ Department of Physics, Pohang University of Science and Technology, 169-148 Gwahak-ro, Pohang, Gyeongbuk, 37673, Republic of Korea

E-mail: reman.bernard-charles-g@warwick.ac.uk

Received 29 August 2021, revised 25 May 2022

Accepted for publication 14 June 2022

Published 29 June 2022



CrossMark

Abstract

During bursty MHD events, transient ion cyclotron emission (ICE) is observed from deuterium plasmas in the large helical device (LHD) heliotron-stellarator. Unusually, the frequencies of the successive ICE spectral peaks are not close to integer multiples of the local cyclotron frequency of an energetic ion population in the likely emitting region. We show that this ICE is probably driven by a subset of the fusion-born protons near their birth energy $E_H = 3.02$ MeV. This subset has a kinetic energy component parallel to the magnetic field, $m_H v_{\parallel}^2/2$, significantly greater than its perpendicular energy $m_H v_{\perp}^2/2$, for which $v_{\perp} \sim V_A$, the Alfvén speed. First principles computations of the collective relaxation of this proton population, within a majority thermal deuterium plasma, are carried out using a particle-in-cell approach. This captures the full gyro-orbit kinetics of all ions which, together with an electron fluid, evolve self-consistently with the electric and magnetic fields under the Maxwell–Lorentz equations. The simulated ICE spectra are derived from the Fourier transform of the fields which are excited. We find substantial frequency shifts in the peaks of the simulated ICE spectra, which correspond closely to the measured ICE spectra following the resonance condition $\omega = k_{\parallel} v_{\parallel} + n\Omega_H$ for n th proton harmonic. This suggests that the transient ICE in LHD is generated by the identified subset of the fusion-born protons, relaxing under the magnetoacoustic cyclotron instability. So far as is known, this is the first report of a collective radiation signal from fusion-born ions in a

⁸ Formerly at ONERA–The French Aerospace Lab, Toulouse 31055, France.

⁹ Now at General Atomics, San Diego, CA, United States of America.

¹⁰ Now at Institute of Advanced Energy, Kyoto University, Gokasho, Uji, Kyoto 611-0011 Japan.

* Author to whom any correspondence should be addressed.



Original Content from this work may be used under the terms of the [Creative Commons Attribution 4.0 licence](https://creativecommons.org/licenses/by/4.0/). Any further distribution of this work must maintain attribution to the author(s) and the title of the work, journal citation and DOI.

non-tokamak magnetically confined plasma. Disambiguation between two or more energetic ion species that could potentially generate complex observed ICE spectra is an increasing challenge, and the results and methodology developed here will assist this. Our approach is also expected to be relevant to ICE driven by ion beams with lower parallel velocities, for example in cylindrical plasma experiments.

Keywords: large helical device, fusion-born ions, ion cyclotron emission, hybrid kinetic modelling, high performance computing, heliotron stellarator

(Some figures may appear in colour only in the online journal)

1. Introduction

The initial deuterium plasma campaign [1–8] on the large helical device (LHD) heliotron-stellarator has provided interesting new opportunities to study the fundamental physics of ion cyclotron emission (ICE) [9, 10]. ICE was detected both during perpendicular deuterium neutral beam injection (NBI) [11–15] and during transient events. In this paper, we focus on the ICE that arises during transient events [16–22] which may be caused by the helically trapped energetic-ion-driven resistive interchange MHD mode (EIC), characterised by the mode numbers $m = 1$ and $n = 1$ (poloidal and toroidal respectively) [16–19]. The abrupt onset of an associated tongue-shaped magnetic surface deformation has been reported in LHD [21–23]. Contemporaneously, brief intense RF signals are detected in the hundreds of megahertz range. These signals exhibit successive ICE spectral peaks which have a typical frequency spacing of 20 MHz to 25 MHz, comparable to the proton cyclotron frequency. Importantly, these peaks are not located close to integer cyclotron harmonics. This is in contrast to ICE spectra from LHD where the spectral peaks are very close to successive ion cyclotron harmonics, driven by hydrogen (deuterium) NBI in hydrogen (deuterium) plasmas, see [11–15].

In this paper we argue that the ultimate origin of the transient ICE with spectral peaks highly shifted with respect to cyclotron harmonics lies in the fusion reactions within deuterium plasmas in LHD, which generate protons with birth energy $E_H = 3.02$ MeV. We propose here that a subset of these protons, with super-Alfvénic parallel velocities, are responsible for the transient ICE signal (shown, for example, in figures 1 and 2) that is observed during the bursting events outlined above. We arrive at this conclusion notwithstanding that the relative concentration of energetic fusion-born ions n_{energ}/n_e is very low, less than 10^{-7} . As we now briefly review, there are strong experimental precedents for the generation and detection of ICE from fusion-born ions at very low concentrations, comparable to those in LHD deuterium plasmas.

The first measurements of ICE from fusion-born protons in a deuterium plasma were from: JET Ohmically heated tokamak plasmas with currents as low as 1 MA, see the ICE spectra in figure 2 of [9]; and a 3 MA JET plasma heated with 4 MW of 55 keV proton NBI inclined at 58 degrees to the magnetic axis, see figure 1 of [9]. In these plasmas, the overall fusion reaction rate inferred from 2.5 MeV neutron fluxes ranged from 10^{12} s⁻¹ at 1 MA to 10^{14} s⁻¹ at 5 MA [9]. The core plasma electron density was a few times 10^{19} m⁻³ and the confinement time

of energetic ions was a few times 0.1 s, implying a relative concentration of energetic ions $\leq 10^{-7}$. In the first measurements of ICE from fusion-born alpha-particles in deuterium-tritium plasmas in JET, the ratio of local alpha-particle number density to local electron density was inferred from measured neutron fluxes and TRANSP computations. Its value ranged between 10^{-3} at the core and 10^{-5} at the edge, see figure 7 of [10] and the discussion in section 3.3 thereof. The ICE phenomenology broadly resembled that from the prior deuterium plasma experiments at lower energetic ion concentration, see especially figures 2 and 5 of [10]. We note that figure 5 records ICE from Ohmic deuterium plasmas with measured neutron fluxes (and, by extension, approximate energetic ion concentrations) a million times lower than in the deuterium-tritium plasmas. Recent measurements of ICE from a subset of the fusion-born protons in KSTAR deuterium plasmas [24–26] and subsequent interpretation [27, 28] came as a surprise, because it was previously supposed that the fusion-born proton population was zero for all practical purposes, on the basis of plasma parameters and especially of particle orbits in relation to system size. In deuterium tokamak plasma discharges in JT-60U, ICE owing to fusion-born protons was detected [29, 30] during perpendicular and tangential deuterium NBI.

There is thus a strong experimental record of ICE detection from fusion-born ions in plasmas where the fusion-born ion concentration is very low ($\leq 10^{-7}$), or indeed had previously been considered negligible. In this paper we therefore investigate how the ICE signals in figures 1–3 may be excited by a subset of the diffuse population of fusion-born protons, and identify the likely physical origin of its distinctive frequency shift [30, 31]. We carry out direct numerical simulations using a hybrid particle-in-cell (PIC) approach [32–35]. Our computations follow the full gyro-orbit kinetics of hundreds of millions of ions, including both minority energetic ions (protons at 3.02 MeV) and majority thermal deuterons, together with an electron fluid, evolving self-consistently with the electric and magnetic fields under the Maxwell–Lorentz system of equations. The simulation domain spans one spatial axis and all three velocity coordinates (1D3V).

This PIC-hybrid approach was recently applied successfully to the interpretation of ICE from NBI protons in hydrogen and deuterium plasmas in LHD [14, 15]. In related work, the applicability of PIC computations for interpreting ICE from a subset of fusion-born protons in deuterium plasmas was recently demonstrated for KSTAR observations [27, 28], and also for ICE driven by NBI deuterons in KSTAR deuterium plasmas [36], and more recently to ICE emitted

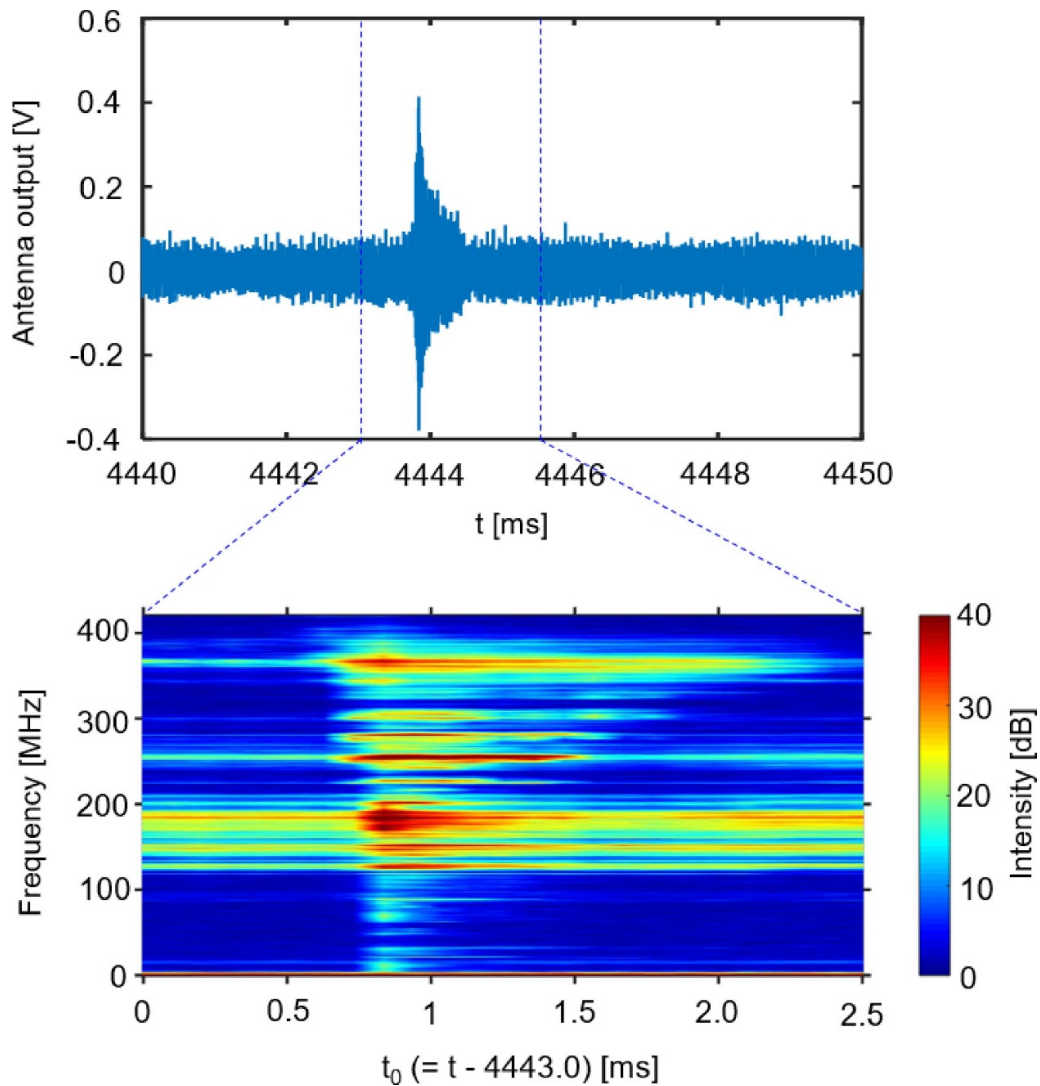


Figure 1. ICE phenomenology measured during the bursty MHD event in LHD deuterium plasma 133979. (Top) Time series of the electric field fluctuations (V). (Bottom) Corresponding windowed Fourier transform showing the time evolution at higher resolution of the frequency content in the hundreds of MHz.

from the core of ASDEX-U [37–40]. In most contemporary ICE measurements, as in the early ICE observations in JET [10] and TFTR [41], the experimentally observed ICE spectral peaks are close to the cyclotron frequency of the energetic ions in the emitting region in the outer midplane plasma. In the corresponding PIC and PIC-hybrid computations [14, 15, 27, 28, 34–36, 40, 42–44], the minority energetic ion population is initialised with a physically motivated non-Maxwellian distribution in velocity space. This population then relaxes collectively under the magnetoacoustic cyclotron instability (MCI) [34, 35, 42, 45–54], which in these simulations manifests at the level of the Maxwell–Lorentz dynamics of the individual particles and the self-consistent fields. The spatiotemporal Fourier transforms of the excited electric and magnetic fields that arise in the PIC-based computations then yield simulated ICE spectra, which compare well with observations.

Identification of the initial distribution in velocity space of the candidate ICE-generating energetic ion population,

prior to relaxation under the MCI, is central to this PIC-based approach. It typically rests on particle orbit studies, for example figure 14 of [10], figure 2 of [52], figure 2 of [27], figure 3 of [36] and [55, 56]. Here we examine the hypothesis that the bursting ICE signal is caused by a single energetic ion population (freshly fusion-born protons) at a single location (inferred from magnetic field strength assuming ion cyclotron phenomenology), operating under a single collective plasma physics process (the MCI). The work which follows shows that this hypothesis may well be valid, and this tends to weigh against more complex hypotheses involving a greater number of entities, for example more than one driving ion species at more than one location. For the present application, we develop, as follows, our hypothesis for the velocity space distribution of the emitting sub-population of the protons recently born in deuterium fusion reactions with energy $E_H = 3.02$ MeV. We first assume that, as usual, this ICE is dominated by waves propagating close to perpendicular to the local background magnetic field, and which are excited by

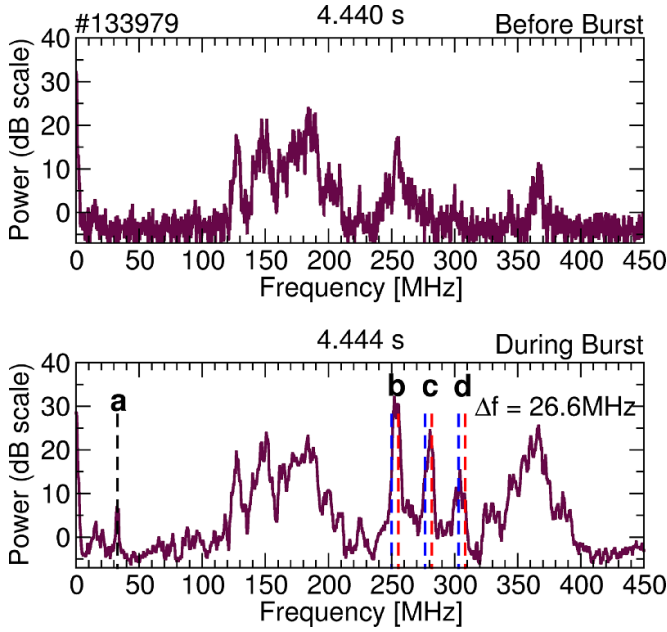


Figure 2. ICE power spectra from LHD plasma 133979 before (top panel) and during (bottom) the bursty MHD event. The spectrum at the time of the bursty event exhibits three intense peaks *b*, *c* and *d*, together with peak *a*, and there is additional activity above 300 MHz. The peaks *b*, *c*, *d* are located between 250.04 and 255.36 MHz, between 276.64 and 281.96 MHz, and between 303.24 and 308.56 MHz. The shifted harmonics of $26.6 \times (n - 0.6)$ are indicated with blue dashed lines for $n = 10, 11, 12$ and shifted harmonics of $26.6 \times (n + 0.6)$ are indicated with red dashed lines for $n = 9, 10, 11$ respectively; peak *a* is at 32.73 MHz.

the MCI of a highly non-Maxwellian energetic ion population. Specifically, these waves are on the fast Alfvén-cyclotron harmonic wave branch; this follows from the analytical theory of the MCI [45–54, 57], and is confirmed by analysis of the oscillations self-consistently excited in first principles PIC-based computations [14, 15, 27, 28, 34–36, 40, 42–44, 58]. We assume that the ICE is primarily driven by a sub-population of energetic ions, which we can model approximately in terms of a drifting-ring velocity distribution [59]:

$$f(v_{\parallel}, v_{\perp}) = \frac{n_{\text{energ.}}}{2\pi v_{\perp}} \delta(v_{\perp} - u_{\perp}) \delta(v_{\parallel} - u_{\parallel}), \quad (1)$$

whose free parameters are its density $n_{\text{energ.}}$, u_{\perp} and u_{\parallel} . On the basis of many previous studies of ICE and its driving instability, the MCI [14, 34, 35, 41, 50, 52, 57, 60], we fix u_{\perp} to be close to the local Alfvén speed V_A , because this is a preferred, but not a necessary, condition for ICE to be strongly driven. The centrality of the condition $u_{\perp} \sim V_A$ has been re-emphasised by recent analytical and numerical studies [44, 61]. We assume that the driving ions are fusion-born protons at their birth energy $E_H = 3.02$ MeV, and note that ICE unfolds on μs timescales during which no significant collisional energy loss has had time to occur. Their parallel component of kinetic energy follows from:

$$u_{\parallel}^2 = \frac{2}{m_H} E_H - u_{\perp}^2. \quad (2)$$

This defines a value for $u_{\parallel} > u_{\perp} \approx V_A$ which, when used in the PIC computations, gives rise to substantial spectral shifts in the simulated spectra. We shall show that these shifts correspond closely to the measured differences between ICE spectral peak frequencies and the integer harmonics of the local proton cyclotron frequency, that are observed during the transient events in LHD [16, 17, 21–23]. This tends to confirm our identification of this particular subset of the fusion-born protons, near their birth energy, as a candidate energetic ion population responsible for the bursting ICE.

An alternative scenario reported in [62] suggests that 178 keV NBI protons, injected tangentially with low pitch angle, could also excite ICE with a spectrum displaying a substantial frequency shift from integer cyclotron harmonics. This approach differs from the one explored in this paper, in that the free energy available to destabilise electromagnetic waves is much lower than for the 3.02 MeV fusion-born protons we consider here. The lower velocities v_{\parallel} together with higher k_{\parallel} [62] result in $k_{\parallel} v_{\parallel}$ being a small fraction of the proton cyclotron frequency Ω_H when considering the resonant condition of the n th proton cyclotron harmonic including Doppler shift:

$$\omega = k_{\parallel} v_{\parallel} + n\Omega_H. \quad (3)$$

Conversely the concentration of energetic ions $n_{\text{energ.}}/n_e$ is much higher for the NBI case; it is of order 5% for NBI protons in [62], whereas $n_{\text{energ.}}/n_e$ is estimated to be of the order of 10^{-7} for fusion-born protons in LHD. However, as we have reviewed earlier in this section, ICE driven by fusion-born ions at very low concentrations $\leq 10^{-7}$ is a well established experimental phenomenon in tokamak plasmas.

The present study is topical, in that recent observations from ASDEX-Upgrade [37] and DIII-D [63–65] exhibit increasing diversity and complexity in the distribution of ICE spectral peaks. There may be multiple candidate energetic ion species, both fusion-born and NBI, either sub- or super-Alfvénic, furthermore ICE is detected from the core plasma [38, 39], as well as from its traditional locus near the outer midplane edge [13, 64]. This disambiguation is addressed in relation to contemporary ICE observations in the ASDEX-Upgrade tokamak [37–40, 61]. Distinction between NBI drive and fusion-ion drive of ICE in early JET deuterium plasmas was achieved by observing ICE spectra for otherwise similar plasmas with widely different core density (and hence fusion reactivity) and the same NBI power, see figure 2 of [9]. This comparison might be more difficult to achieve in deuterium plasmas in LHD, which was not designed on a scale to achieve comprehensive energetic ion confinement. Frequency shifts of the kind examined here introduce a further degree of freedom to the frequency at which ICE spectral peaks are observed [29, 31, 50, 52, 53]. There is thus a new challenge, which one might term ICE plasma chemistry, in identifying the most likely ICE-generating ion species, together with their locations, from contemporary observed spectra where these are not immediately obvious. The localisation of the ICE-generating subset in velocity space, which follows from the present analysis of the LHD data presented in figures 1 and 2, provides

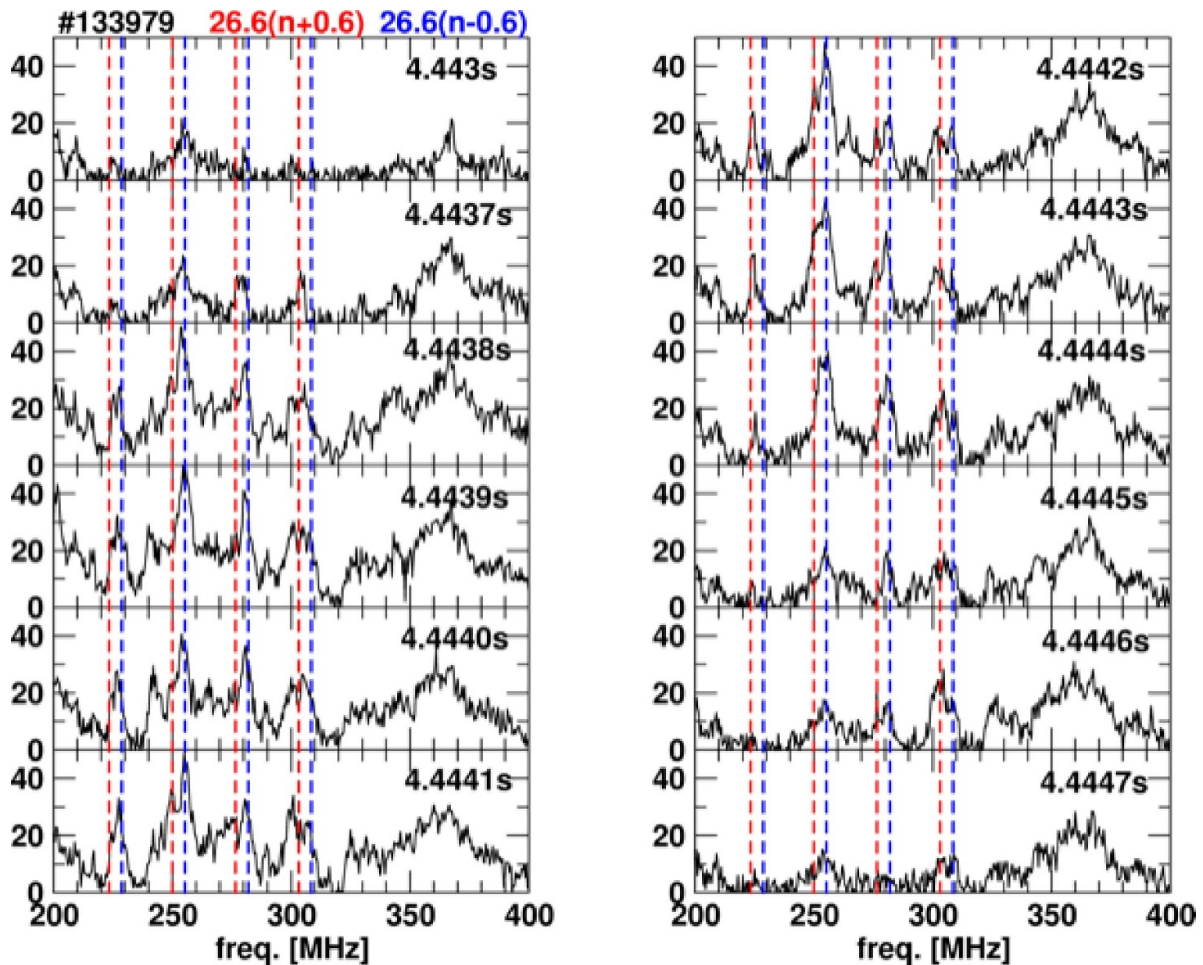


Figure 3. Measured power spectra in LHD plasma 133979 taken at several successive times between $t = 4.4430$ s and $t = 4.4447$ s in the magnetic configuration $(R_{ax}, B_{toroidal}) = (3.6 \text{ m}, 2.75 \text{ T})$. The panel at $t = 4.4430$ s corresponds to the spectrum before the burst occurrence. The blue dashed vertical lines correspond to $n = 26.6 \times (n + 0.6)$ MHz, $n = 8, 9, 10, 11$. The red dashed vertical lines correspond to $n = 26.6 \times (n - 0.6)$ MHz, $n = 9, 10, 11, 12$.

an example of the reconstruction of the zeroth-order features of the velocity space distribution function of an energetic ion population, based solely on ICE measurements [59, 66–69]. In a recent development, this is being further examined using neural networks [70]. This in turn illustrates the diagnostic potential of ICE [71].

2. Observations of ICE during transient events in hydrogen and deuterium plasmas in LHD

2.1. ICE measurement system

The ICE acquisition system on LHD uses a dipole antenna developed in partnership with KSTAR [72–74]. The measurement system comprises a dipole antenna located in the 10-O port of LHD, inside the vacuum vessel whose centre is very close to the equatorial plane, about one degree below it. A fast digitizer performs direct sampling of the radiofrequency measurements at $1.25 \text{ GSamples s}^{-1}$. The time evolution of the RF signal intensity is collected by a 14-channel filter bank spectrometer in the range of 70–2800 MHz, with intermediate spectral resolution and with μs time resolution for a duration spanning

the whole plasma discharge [74]. A ‘discone’ antenna, which is a type of dipole antenna designed to detect waves in the radiofrequency range 100–2500 MHz, is also installed in the 9.5-L port of LHD inside the vacuum vessel, and the detected signal is acquired with a fast digitizer at $12.5 \text{ GSamples s}^{-1}$ for 80 ms. The locations of tangential and perpendicular NBIs and RF antennas are shown in figure 4.

2.2. Previous observations from Hydrogen plasmas in LHD

In order to isolate the potential role of fusion-born protons in the ICE from LHD deuterium plasmas which is our main focus in this paper, it is first necessary to consider the potential role of NBI ions. Observations from earlier hydrogen plasmas in LHD can shed light on this, as follows. In some LHD hydrogen plasmas, transient events with bursty fluctuations were observed both as magnetic probe signals and as radiofrequency signals during heating by perpendicular NBI #4 and #5, as shown in figures 5(a)–(c).

On the other hand, without NBI #4, the bursty fluctuations appear only in the radiofrequency signal detected by the discone antenna as shown in figures 6(a)–(c).

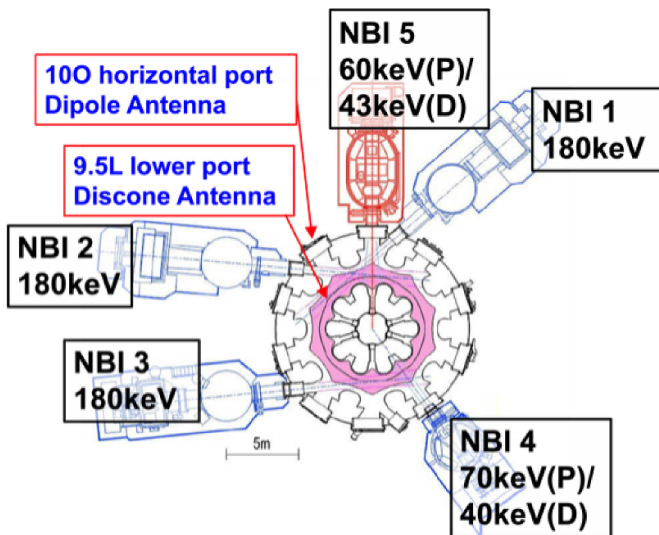


Figure 4. Locations of NBIs and RF (dipole and discone) antennas. These are shown together with the typical values of the beam energy of each NBI.

These plasmas were heated by tangential neutral proton beams at 186 keV (NBI #1), 170 keV (NBI #2), 170 keV (NBI #3), and by perpendicular proton beams at 43 keV (NBI #4), 40 keV (NBI #5). The magnetic configuration of these plasmas was $(R_{ax}, B_t) = (3.600 \text{ m}, 2.850 \text{ T})$ where R_{ax} is the distance between the centre of the torus and the magnetic axis, and B_t is the magnetic field strength at the magnetic axis. The corresponding spectrograms displaying the radiation power of the radio frequency waves detected by the discone antenna are shown in figure 7 for discharges with and without NBI #4. Unfortunately, the fast digitizer did not acquire the signal detected by the dipole antenna at this time. Figure 8 shows the frequency spectra before and during the burst with and without NBI #4. As shown in the upper left panel of figure 7 and in the upper panel of figure 8 corresponding to LHD hydrogen plasma 129564, radiation in the frequency range of $100 \text{ MHz} < f < 350 \text{ MHz}$ is strongly enhanced during the burst when NBI #4 is applied. The enhanced signal in the frequency range between 200 MHz and 300 MHz spans the 7th–12th harmonics of a fundamental frequency considered to lie in the interval 28.22–29.55 MHz, as shown in the upper panel of figure 8. As indicated in figure 9, the fundamental proton cyclotron resonances of 28.22–29.55 MHz are located near the last closed flux surface (LCFS), which is defined as $r_{eff}/a_{99} = 1$, where r_{eff} is the effective minor radius, such that 99% of the electron kinetic energy in the plasma lies within $r_{eff} = a_{99}$. Conversely, the radiation in the frequency range $325 \text{ MHz} < f < 350 \text{ MHz}$ only is strongly enhanced when NBI #4 is not operated, as indicated on the right panel of figure 7 and in the lower panel of figure 8 which corresponds to LHD hydrogen plasma 129574. The profiles of electron density and electron and ion temperatures plotted versus the normalised minor radius defined by r_{eff}/a_{99} are similar to each other as shown in panels (e) and (f) of figures 5 and 6. These results from hydrogen plasmas suggest that emissions in the

range of 200–300 MHz emitted near the LCFS following the burst originates from high energy protons supplied by perpendicular NBI and not by tangential NBI.

2.3. Observations of bursting ICE from LHD deuterium plasma

In LHD deuterium plasmas that are otherwise similar to the hydrogen plasmas discussed above, transient events with bursty fluctuations were observed in both magnetic fluctuations and radiofrequency signals during heating with perpendicular NBI #4 and #5, as shown in the panels (b) and (c) of figure 10. The magnetic configuration of this discharge was $(R_{ax}, B_t) = (3.600 \text{ m}, 2.750 \text{ T})$ and the plasma was heated by tangential NB proton beams at 185 keV (NBI #1), 162 keV (NBI #2), 175 keV (NBI #3), and perpendicular NB deuterium beams of 59 keV (NBI #4), 70 keV (NBI #5). A distinctive ICE signal, in the frequency range between 200 MHz and 300 MHz, was detected during a transient event with bursty fluctuations in LHD deuterium plasma 133979. The measured perturbed electric field time series shown in figure 1 has spectral peaks (see also figure 2) whose separation could be related to the cyclotron frequency of an energetic ion species: in particular, the 3.02 MeV fusion-born protons, born in deuterium-deuteron fusion reactions. As we describe below, these spectra are different from ICEs observed in hydrogen discharge and ICEs previously investigated. First, the peaks appear to have undergone substantial Doppler shifts with respect to local integer cyclotron harmonics; and second, the frequency interval between successive peaks is not strictly uniform. As an example of this ICE phenomenology, the top panel of figure 1 shows the time series of the electric field intensity of the bursting ICE at $t \approx 4.443 \text{ s}$ in LHD plasma 133979, and the bottom panel shows the corresponding spectrogram displaying intense radio frequency activity in the hundreds of megahertz range with increasingly high time resolution. We shall show that these effects can arise naturally from the substantial super-Alfvénic parallel velocity of the energetic protons that, we argue, drive this ICE. Figure 2 presents two ICE power spectra, taken (top) just before the bursty event at $t = 4.440 \text{ s}$, and (bottom) during the event at $t = 4.444 \text{ s}$. The major difference consists in the appearance during the burst of the three peaks labelled *b*, *c*, *d* in the lower panel, together with peak *a*. The spectral peaks *b*, *c*, and *d*, are located between 250.04 and 255.36 MHz (*b*), between 276.64 and 281.96 MHz (*c*), and between 303.24 and 308.56 MHz. Here, the lower limits 250.04, 276.64, and 303.24 MHz can be written $26.6(n - 0.6)$ MHz for $n = 10, 11, 12$. The upper limits at 255.36 MHz, 281.96 MHz and 308.56 MHz, can be written $26.6(m + 0.6)$ MHz for $m = 9, 10, 11$. The shift of $\pm 0.6 \times 26.6 \text{ MHz}$ corresponds closely to the Doppler shift due to large v_{\parallel} of fusion-born protons. Fusion-born ions are distributed randomly and uniformly with respect to solid angle in velocity-space at birth, hence v_{\parallel} can have both positive and negative values. Therefore the lead hypothesis, whose physical consistency we explore in this paper, is that this ICE is generated locally at the Doppler-shifted proton cyclotron resonance whose fundamental frequency is 26.6 MHz. Figure 10(a) displays the time evolution

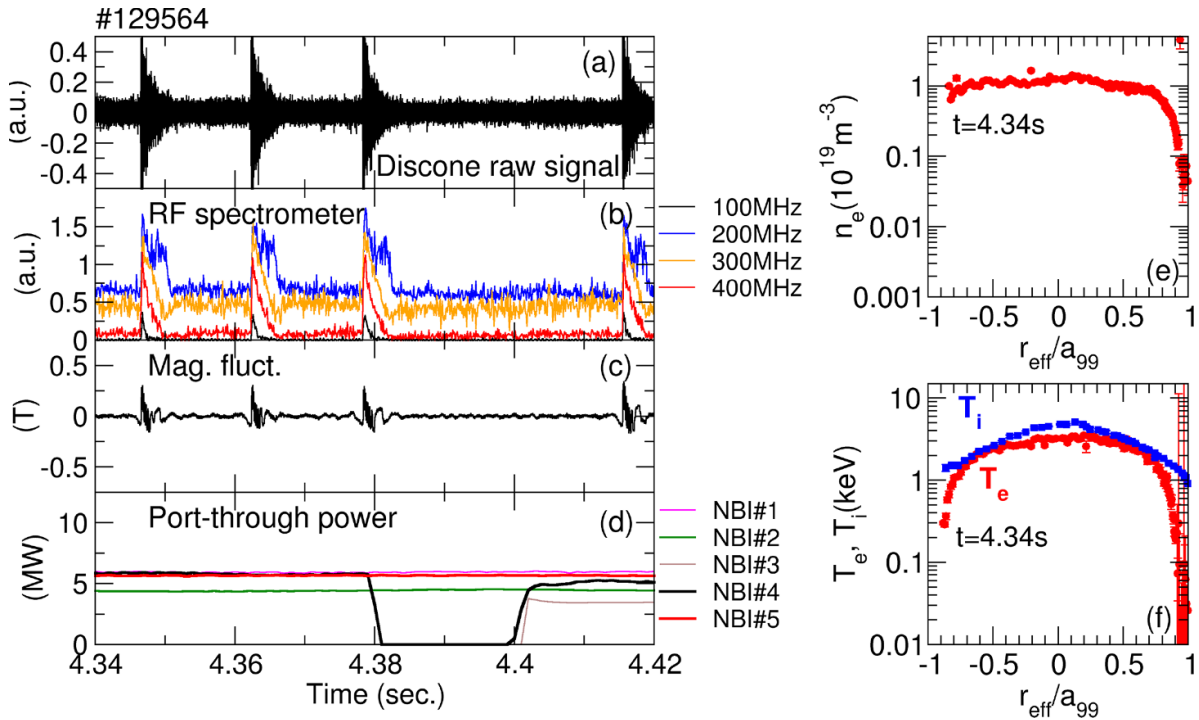


Figure 5. Evolution of plasma parameters in LHD hydrogen plasma 129564 during which NBI #4 is turned off between $t = 4.38$ s and $t = 4.40$ s. Time traces of (a) electric field fluctuations detected by the discone antenna, (b) emission intensities detected by the RF spectrometer, (c) magnetic field fluctuations detected by magnetic probe (d) NBI port through power, and radial profiles of (e) electron density, (f) electron and ion temperatures.

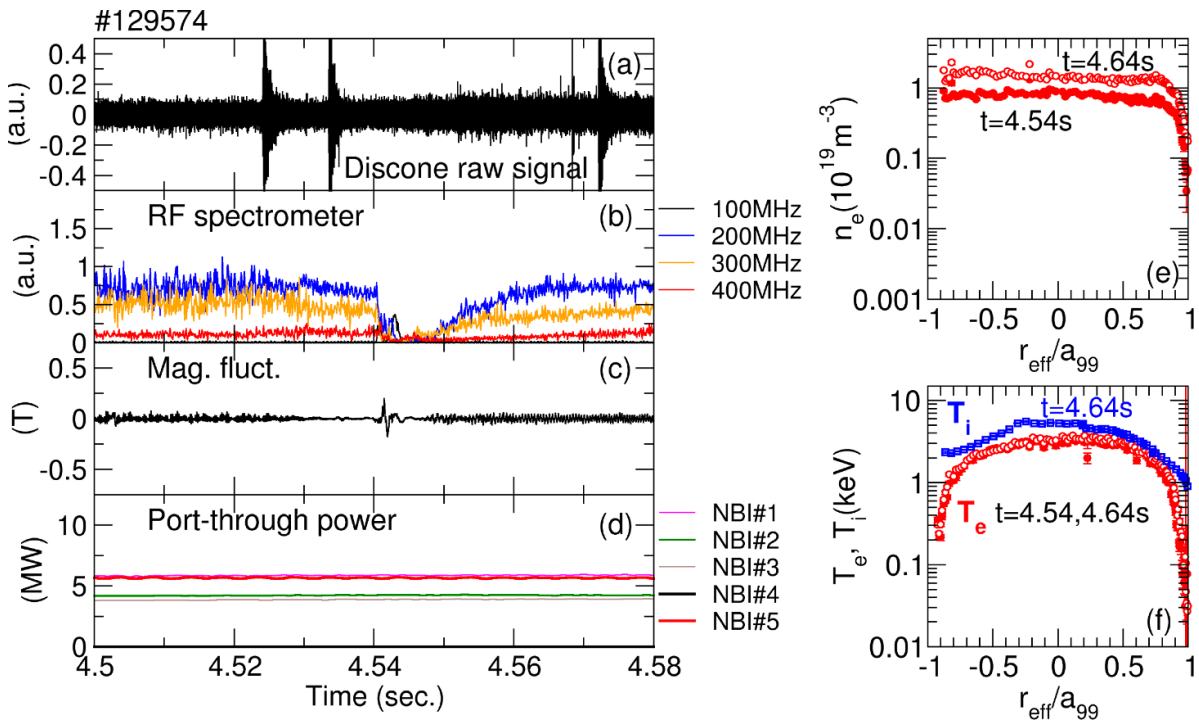


Figure 6. Evolution of plasma parameters in LHD hydrogen plasma 129574 during which NBI #4 is not operated throughout the whole duration of experiment. The time traces and radial profiles are similar to those of figure 5.

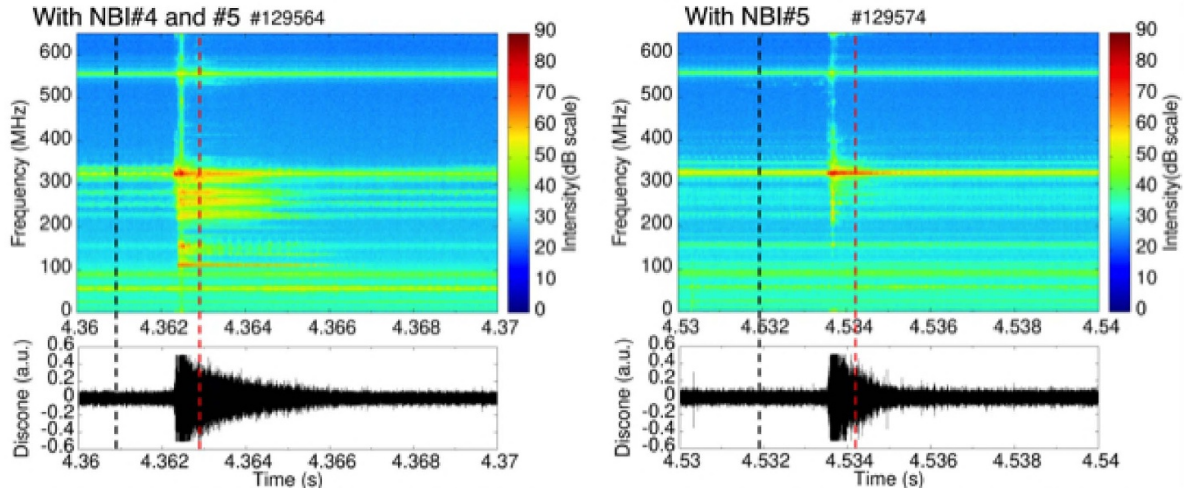


Figure 7. Frequency spectrograms (upper panels) obtained by FFT analysis of the electric field fluctuations (lower panels) surrounding two bursty events in LHD hydrogen plasmas. (Left panels) Plasma 129564 heated by both NBI #4 and #5. (Right panels) Plasma 129574 heated only by NBI #5. The red and dark vertical lines show the times at which the ICE spectra shown in figure 8 are taken.

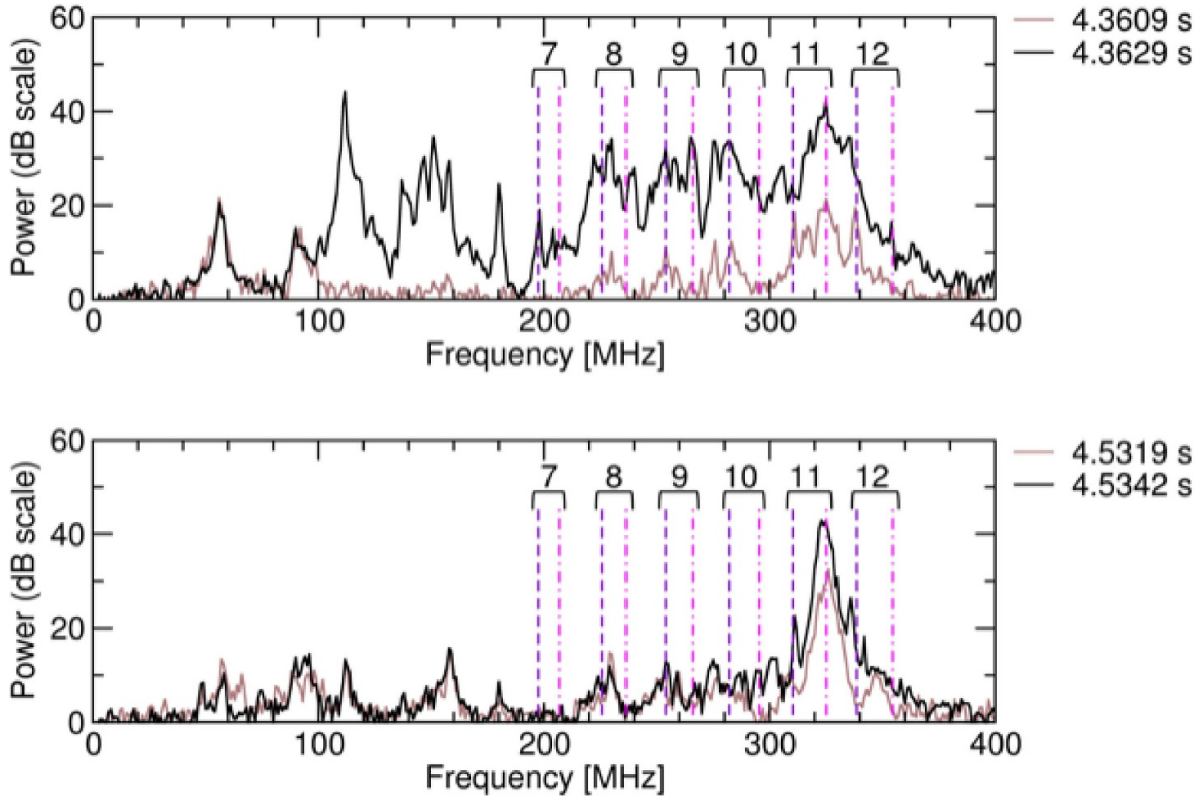


Figure 8. Power spectra offset by the noise level taken before (brown solid line) and during (black solid line) the bursty events observed with NBI #4 (upper panel), and without NBI #4 (lower panel) in LHD hydrogen plasmas 129564 and 129574 respectively. The dashed vertical lines represent the locations of the 7th–12th harmonics of 28.22 MHz (violet) to 29.55 MHz (magenta).

of the measured neutron flux between $t = 4.41$ s and $t = 4.49$ s during deuterium discharge of LHD plasma 133979. Over this discharge, the neutron flux reaches its maximum value in this time range as shown in figure 10. The neutron flux increases until the occurrence of the bursty event, and decreases following it [6]. This must result in a transient surge in the number of fusion-born protons at 3.02 MeV, implying a transient

inversion (local positive slope) of the velocity-space distribution of the protons, which is necessary for them to be able to drive ICE. Figure 10(d) shows that the NBI power is steady around the time of the burst. Figure 10(b) plots the time evolution of the power radiated by the plasma in six different radio frequency channels, between 100 and 400 MHz. Intense transient activity is visible. Moreover, similar transient activity is

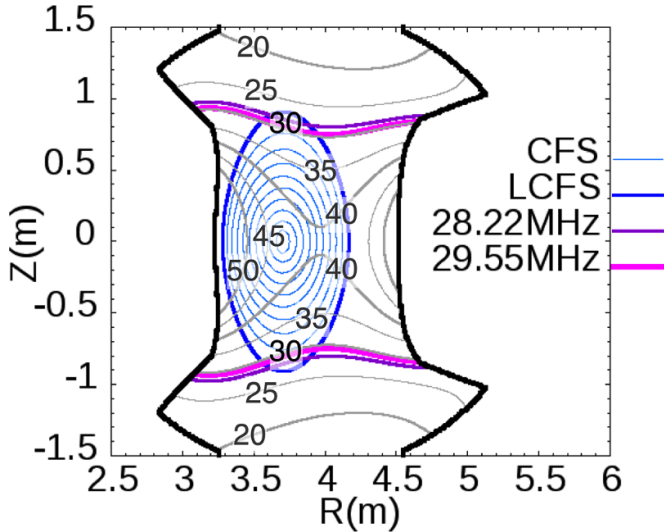


Figure 9. Contours of the proton cyclotron frequency with 5 MHz interval (grey lines), contours of the closed magnetic flux surfaces (blue lines), locations of the fundamental proton cyclotron resonances of 28.22 MHz (purple line) and 29.55 MHz (magenta lines) at the vertically long cross section where the discone antenna is installed in the lower port.

observed in frequency channels of 600 and 800 MHz, however the origin of the activity in these highest observed frequencies are not clear. In the present paper, we focus on the energetic ion physics underlying the radio frequency bursts in the range 200–300 MHz. The generation mechanism of these bursts could lie in the interplay between a quasi stable stationary (non-rotating) 1/1 MHD mode, a tongue-shaped deformation of the plasma at a non rational surface and a rotating 1/1 mode with MHD bursts [23]. As the tongue-shaped deformation arises, it hinders the stationary 1/1 mode and draws on the free energy of the instability which lies in the strong gradient of energetic ions. The tongue deformation results most likely from the pressure gradient of the trapped ions supplied by the NBI. A strong RF signal at a frequency ≈ 800 MHz accompanies the collapse along with RF signals which are observed in the frequency range between 200 and 300 MHz during both MHD activity and tongue-shaped deformation (see bottom of figure 2 in [23]).

There are some notable apparent parallels between recent ICE measurements from NSTX-U and the observed link between the LHD bursting ICE locale and the ‘Tongue’ that we report here. Submillisecond bursts of ICE driven by marginally super-Alfvénic NBI deuterons in NSTX-U were observed [75] to be spatially colocated with internal transport barriers that are well within (by tens of centimetres) the plasma. Figures 4 and 5 of [75] display striking measurements of the correlation of the gently time-varying radial location of the ICE emission with the location where contours of electron density are concentrated, together with the steep ion temperature gradient. The experimental results from the present paper thus share several intriguing physical features with the results reported in [75]. Both relate to bursting ICE driven by a super-Alfvénic ion species—fusion-born protons in LHD and NBI deuterons

in NSTX-U; and the location of the ICE in both cases correlates with a strongly nonlinear feature of the plasma—the ‘Tongue’ in LHD [23] and the internal transport barrier in NSTX-U.

3. Identification of the candidate sub-population of fusion-born protons

The redistribution of the initially helically-trapped ions that are implicated in burst kinetic MHD [16, 17, 19] or abrupt tongue deformation [21, 22] could generate a distinct, transient, highly non-Maxwellian distribution in velocity space, perhaps involving the expelled ions and freshly trapped ions. Let us therefore make the assumption (for this, or some as-yet-unknown, reason) that a transient, spatially localised, highly non-Maxwellian population of 3.02 MeV fusion-born protons could be responsible for the ICE spectral peaks *b*, *c* and *d* in figure 2. Our initial goal is then to perform multiple PIC-hybrid computations of the collective relaxation of these highly energetic protons, using the plasma parameters at an appropriately inferred ICE emission location; and to investigate whether the resulting simulated ICE power spectra are compatible with the measurements in figure 2. In this section, we identify the fundamental cyclotron frequency with the mean frequency spacing between the peaks *b*, *c* and *d*. This allows us to determine the emission location and thus the plasma parameters necessary to initialise our simulations in section 4. This approach assumes that these peaks have a common emission location. If the radiation is generated by protons, identifying the 26.6 MHz mean frequency spacing between these peaks as an indicative local proton cyclotron frequency implies a local magnetic field strength of 1.75 T. As shown in figure 11, the corresponding proton cyclotron resonance on the midplane is located at $R = 4.521$ m that corresponds to the normalised minor radius $r_{\text{eff}}/a_{99} = 0.956$ and is close to the LCFS at the horizontally long poloidal cross section where the dipole antenna is installed. As indicated in figures 10(e) and (f), the electron and ion temperatures at $r_{\text{eff}}/a_{99} = 0.956$ are 846 eV and 907 eV respectively, while the electron number density is $8.8 \times 10^{18} \text{ m}^{-3}$ such that $V_A = 0.9105 \times 10^7 \text{ ms}^{-1}$; these are used as input parameters in our PIC-hybrid simulations. The rotation flow velocity of the LHD plasma is around 10^4 ms^{-1} and is negligibly small compared to the order of the Alfvén velocity.

Table 1 gives the computed time after which 3.02 MeV protons are lost, as a function of their radial birth location and of their initial pitch angle, evaluated in the equatorial plane of LHD. The red boxes are the initial locations corresponding to unconfined fusion-born protons. Conversely, there is the possibility for fusion-born protons to remain on confined trajectories [76]. The ICE-relevant density of the fusion-born protons n_H can be evaluated by integration over the restricted range of pitch angle values, α , that contribute to exciting the MCI. We can estimate n_H from the expression:

$$n_H = \text{fac}(FC \times t_{st})/V = \text{fac} \times 10^{12} \text{ m}^{-3}, \quad (4)$$

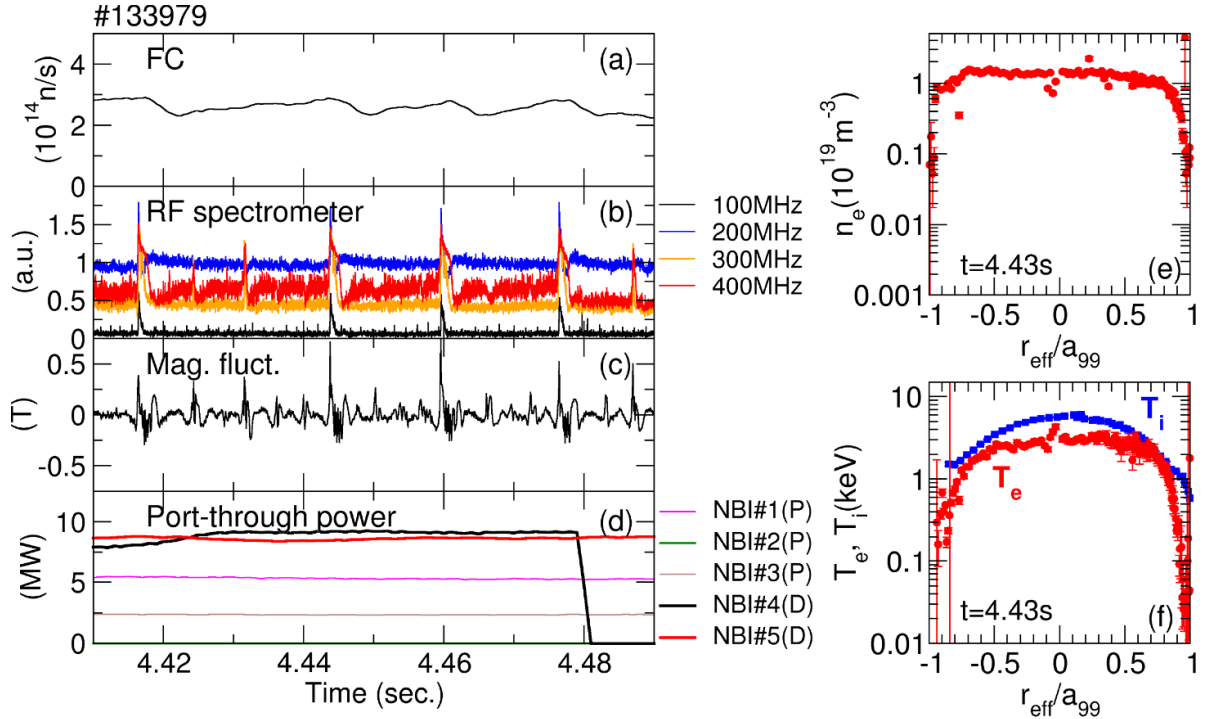


Figure 10. Time evolution of plasma parameters in LHD deuterium plasma 133979. Time traces of (a) neutron flux, (b) emission intensities from the filter bank system (RF spectrometer) detected by 10-O dipole antenna, (c) magnetic fluctuation detected by magnetic probe, (d) NBI port through power, and radial profiles of (e) electron density, (f) electron and ion temperature.

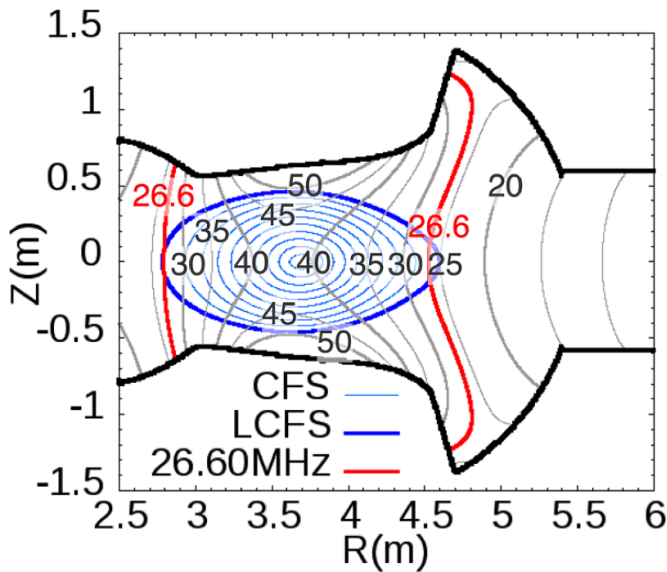


Figure 11. Contours of the proton cyclotron frequency with 5 MHz interval spacing (grey lines), locations of the fundamental proton cyclotron resonance of 26.6 MHz (red lines) and contours of closed magnetic flux surfaces (blue lines) sliced at vertically long poloidal cross section where the dipole antenna is installed.

where t_{sl} is the slowing time indicated inside blue and red boxes in table 1; FC is the neutron flux in neutron s^{-1} ; and V is the plasma volume of LHD. Approximate values for these parameters are $FC = 3.0 \times 10^{14}$, $V = 30 \text{ m}^3$, $t_{sl} = 50 \times 10^{-3}$ s. Hence we may infer the fusion-born ion concentration n_H/n_e is less than 10^{-7} since n_e is of the order of 10^{19} and the factor

value fac is less than 1. Further studies have shown that other particles in the MeV energy range can be confined in LHD [76]. For example, some 15 MeV protons resulting from the $D + {}^3\text{He} \rightarrow {}^4\text{He} (3.67 \text{ MeV}) + p (15 \text{ MeV})$ reaction are confined over the chaotic field line region [77], but these are not obvious candidates to drive the ICE signal from deuterium plasmas considered here.

In order to make use of the information in table 1 to establish whether the candidate ICE-generating protons at the location of the ICE bursts are indeed confined, we need to establish a mapping between particle velocity vectors there and at the birth location. We first calculate the magnetic moment of the potentially confined sub-population of 3.02 MeV fusion-born protons at the burst location, which we denote by:

$$\mu_{ICE} = \frac{m_H v_{\perp, burst}^2}{2|B_{burst}|}. \quad (5)$$

Here the value of $v_{\perp, burst}$, which denotes the perpendicular velocity of the ICE-emitting ions at the burst location, is not exactly known but is strongly constrained, as we describe below; and we assume $|B_{burst}| = |B_{ICE}| = 1.75 \text{ T}$, as already established. We now invoke the conservation of magnetic moment $\mu_{ICE} = \mu_R$, with $\mu_R = m_H v_{\perp, R}^2 / 2|B(R)|$ the magnetic moment at major radius R , where the local perpendicular velocities of the protons is denoted by $v_{\perp, R}$, and the corresponding local magnetic field strength is denoted $|B(R)|$. It follows that:

$$v_{\perp, R} = \sqrt{\frac{2|B(R)|\mu_{ICE}}{m_H}}. \quad (6)$$

Table 1. Table showing the time after which a 3.02 MeV proton born in the horizontally elongated poloidal part of the equatorial plane in LHD is lost as a function of major radial location and pitch angle (defined by equation (8)) at birth. Red boxes denote promptly lost protons and the number inside each indicates the time before loss, in milliseconds. The remaining protons, corresponding to the blue boxes, constitute the local confined population and define its velocity distribution. The underlying calculation [56] tracks the guiding centre and stops at 50 ms which corresponds to the slowing down time. Collisions are neglected because their timescale are long compared to the timescales on which ICE unfolds.

Pitch angle (degrees)	2.7	2.8	2.9	3.0	3.1	3.2	3.3	3.4	3.5	3.6	3.7	3.8	3.9	4.0	4.1	4.2	4.3	4.4	4.5	4.6	4.7	4.8	4.9	5.0
	Radius (m)																							
171	3.88×10 ⁻⁴	1.5×10 ⁻³	5.0×10 ¹	5.0×10 ¹	5.0×10 ¹	5.0×10 ¹	5.0×10 ¹	5.0×10 ¹	5.0×10 ¹	5.0×10 ¹	5.0×10 ¹	5.0×10 ¹	5.0×10 ¹	5.0×10 ¹	5.0×10 ¹	5.0×10 ¹	5.0×10 ¹	5.0×10 ¹	5.0×10 ¹	5.0×10 ¹	5.0×10 ¹	5.0×10 ¹	5.0×10 ¹	5.0×10 ¹
162	4.0×10 ⁻³	1.5×10 ⁻³	5.0×10 ¹	5.0×10 ¹	5.0×10 ¹	5.0×10 ¹	5.0×10 ¹	5.0×10 ¹	5.0×10 ¹	5.0×10 ¹	5.0×10 ¹	5.0×10 ¹	5.0×10 ¹	5.0×10 ¹	5.0×10 ¹	5.0×10 ¹	5.0×10 ¹	5.0×10 ¹	5.0×10 ¹	5.0×10 ¹	5.0×10 ¹	5.0×10 ¹	5.0×10 ¹	5.0×10 ¹
153	4.3×10 ⁻⁴	4.4×10 ⁻³	5.0×10 ¹	5.0×10 ¹	5.0×10 ¹	5.0×10 ¹	5.0×10 ¹	5.0×10 ¹	5.0×10 ¹	5.0×10 ¹	5.0×10 ¹	5.0×10 ¹	5.0×10 ¹	5.0×10 ¹	5.0×10 ¹	5.0×10 ¹	5.0×10 ¹	5.0×10 ¹	5.0×10 ¹	5.0×10 ¹	5.0×10 ¹	5.0×10 ¹	5.0×10 ¹	5.0×10 ¹
144	3.1×10 ⁻⁴	1.5×10 ⁻³	5.0×10 ¹	5.0×10 ¹	5.0×10 ¹	5.0×10 ¹	5.0×10 ¹	5.0×10 ¹	5.0×10 ¹	5.0×10 ¹	5.0×10 ¹	5.0×10 ¹	5.0×10 ¹	5.0×10 ¹	5.0×10 ¹	5.0×10 ¹	5.0×10 ¹	5.0×10 ¹	5.0×10 ¹	5.0×10 ¹	5.0×10 ¹	5.0×10 ¹	5.0×10 ¹	5.0×10 ¹
135	2.9×10 ⁻³	3.0×10 ⁻³	1.1×10 ²	5.0×10 ¹	5.0×10 ¹	5.0×10 ¹	5.0×10 ¹	5.0×10 ¹	5.0×10 ¹	5.0×10 ¹	5.0×10 ¹	5.0×10 ¹	5.0×10 ¹	5.0×10 ¹	5.0×10 ¹	5.0×10 ¹	5.0×10 ¹	5.0×10 ¹	5.0×10 ¹	5.0×10 ¹	5.0×10 ¹	5.0×10 ¹	5.0×10 ¹	5.0×10 ¹
126	2.6×10 ⁻²	5.6×10 ⁻³	3.6×10 ³	1.6×10 ²	5.0×10 ¹	5.0×10 ¹	5.0×10 ¹	5.0×10 ¹	5.0×10 ¹	5.0×10 ¹	5.0×10 ¹	5.0×10 ¹	5.0×10 ¹	5.0×10 ¹	5.0×10 ¹	5.0×10 ¹	5.0×10 ¹	5.0×10 ¹	5.0×10 ¹	5.0×10 ¹	5.0×10 ¹	5.0×10 ¹	5.0×10 ¹	5.0×10 ¹
117	2.5×10 ⁻⁴	5.7×10 ⁻¹	2.4×10 ²	1.8×10 ²	2.5×10 ²	1.2×10 ³	5.0×10 ¹	5.0×10 ¹	5.0×10 ¹	5.0×10 ¹	5.0×10 ¹	5.0×10 ¹	5.0×10 ¹	5.0×10 ¹	5.0×10 ¹	5.0×10 ¹	5.0×10 ¹	5.0×10 ¹	5.0×10 ¹	5.0×10 ¹	5.0×10 ¹	5.0×10 ¹	5.0×10 ¹	5.0×10 ¹
108	2.2×10 ⁻²	8.9×10 ⁻⁴	5.0×10 ¹	1.0×10 ¹	6.3×10 ²	5.0×10 ¹	5.0×10 ¹	5.5×10 ³	5.8×10 ³	1.8×10 ³	1.8×10 ³	1.8×10 ³	3.9×10 ³	1.5×10 ³	1.7×10 ³	1.5×10 ³	1.0×10 ³	4.0×10 ³	4.0×10 ³	4.0×10 ³	4.0×10 ³	4.0×10 ³	4.0×10 ³	4.0×10 ³
99	2.0×10 ⁻²	2.8×10 ⁻⁴	2.0×10 ³	8.0×10 ¹	2.5×10 ¹	1.5×10 ¹	7.5×10 ²	7.5×10 ²	6.2×10 ²	3.2×10 ²	2.7×10 ²	8.7×10 ²	5.0×10 ³	1.1×10 ¹	5.0×10 ¹	5.0×10 ¹	4.3×10 ³	4.5×10 ³	4.5×10 ³	4.5×10 ³	4.5×10 ³	4.5×10 ³	4.5×10 ³	4.5×10 ³
90	1.7×10 ⁻⁴	1.9×10 ⁻⁴	2.8×10 ⁴	1.6×10 ³	9.1×10 ¹	1.25×10 ⁰	8.6×10 ³	3.1×10 ²	3.1×10 ²	1.6×10 ²	3.9×10 ²	8.0×10 ²	1.1×10 ³	3.6×10 ³	1.4×10 ¹	4.9×10 ³	1.9×10 ³	4.3×10 ³	3.6×10 ⁴	3.5×10 ⁴	3.5×10 ⁴	3.5×10 ⁴	3.5×10 ⁴	3.5×10 ⁴
81	1.6×10 ⁻²	1.5×10 ⁻⁴	1.7×10 ⁴	1.7×10 ⁴	2.8×10 ⁴	5.9×10 ¹	3.1×10 ²	6.1×10 ³	5.4×10 ³	5.0×10 ²	7.5×10 ³	1.1×10 ²	1.6×10 ³	1.3×10 ²	4.3×10 ³	3.8×10 ³	3.5×10 ³	3.5×10 ³	3.5×10 ³	3.5×10 ³	3.5×10 ³	3.5×10 ³	3.5×10 ³	3.5×10 ³
72	1.3×10 ⁻²	1.2×10 ⁻⁴	1.7×10 ⁴	1.8×10 ⁴	3.6×10 ⁴	3.1×10 ²	2.3×10 ²	5.0×10 ³	1.5×10 ²	5.0×10 ¹	5.0×10 ¹	5.0×10 ¹	5.0×10 ¹	5.0×10 ¹	5.0×10 ¹	5.0×10 ¹	3.8×10 ³	3.8×10 ³	3.3×10 ⁴	3.3×10 ⁴	3.3×10 ⁴	3.3×10 ⁴	3.3×10 ⁴	3.3×10 ⁴
63	1.2×10 ⁻²	9.5×10 ⁻⁵	1.4×10 ⁴	1.5×10 ⁴	2.1×10 ⁴	1.1×10 ³	6.3×10 ³	5.0×10 ³	5.0×10 ³	5.0×10 ³	5.0×10 ³	5.0×10 ³	5.0×10 ³	5.0×10 ³	5.0×10 ³	5.0×10 ³	4.9×10 ³	4.9×10 ³	3.3×10 ⁴	3.0×10 ⁴	2.8×10 ⁴	2.9×10 ⁴	2.9×10 ⁴	2.9×10 ⁴
54	9.9×10 ⁻²	8.4×10 ⁻⁵	1.2×10 ⁴	1.4×10 ⁴	2.2×10 ⁴	2.2×10 ⁴	5.0×10 ³	5.0×10 ³	5.0×10 ³	5.0×10 ³	5.0×10 ³	5.0×10 ³	5.0×10 ³	5.0×10 ³	5.0×10 ³	5.0×10 ³	5.0×10 ³	5.0×10 ³	4.2×10 ⁴	4.2×10 ⁴	3.2×10 ⁴	3.0×10 ⁴	3.1×10 ⁴	3.4×10 ⁴
45	9.1×10 ⁻²	7.8×10 ⁻⁵	1.0×10 ⁴	2.0×10 ⁴	5.0×10 ⁴	5.0×10 ⁴	5.0×10 ⁴	5.0×10 ⁴	5.0×10 ⁴	5.0×10 ⁴	5.0×10 ⁴	5.0×10 ⁴	5.0×10 ⁴	5.0×10 ⁴	5.0×10 ⁴	5.0×10 ⁴	5.0×10 ⁴	5.0×10 ⁴	5.0×10 ⁴	5.0×10 ⁴	5.0×10 ⁴	5.0×10 ⁴	5.0×10 ⁴	5.0×10 ⁴
36	8.5×10 ⁻²	7.2×10 ⁻⁵	1.1×10 ⁴	8.9×10 ⁴	5.0×10 ⁴	5.0×10 ⁴	5.0×10 ⁴	5.0×10 ⁴	5.0×10 ⁴	5.0×10 ⁴	5.0×10 ⁴	5.0×10 ⁴	5.0×10 ⁴	5.0×10 ⁴	5.0×10 ⁴	5.0×10 ⁴	5.0×10 ⁴	5.0×10 ⁴	5.0×10 ⁴	5.0×10 ⁴	5.0×10 ⁴	5.0×10 ⁴	5.0×10 ⁴	5.0×10 ⁴
27	9.5×10 ⁻²	6.6×10 ⁻⁵	5.0×10 ⁴	5.0×10 ⁴	5.0×10 ⁴	5.0×10 ⁴	5.0×10 ⁴	5.0×10 ⁴	5.0×10 ⁴	5.0×10 ⁴	5.0×10 ⁴	5.0×10 ⁴	5.0×10 ⁴	5.0×10 ⁴	5.0×10 ⁴	5.0×10 ⁴	5.0×10 ⁴	5.0×10 ⁴	5.0×10 ⁴	5.0×10 ⁴	5.0×10 ⁴	5.0×10 ⁴	5.0×10 ⁴	5.0×10 ⁴
18	7.3×10 ⁻²	6.1×10 ⁻⁵	1.7×10 ⁴	5.0×10 ⁴	5.0×10 ⁴	5.0×10 ⁴	5.0×10 ⁴	5.0×10 ⁴	5.0×10 ⁴	5.0×10 ⁴	5.0×10 ⁴	5.0×10 ⁴	5.0×10 ⁴	5.0×10 ⁴	5.0×10 ⁴	5.0×10 ⁴	5.0×10 ⁴	5.0×10 ⁴	5.0×10 ⁴	5.0×10 ⁴	5.0×10 ⁴	5.0×10 ⁴	5.0×10 ⁴	5.0×10 ⁴
9	7.0×10 ⁻²	5.8×10 ⁻⁵	1.6×10 ⁴	5.0×10 ⁴	5.0×10 ⁴	5.0×10 ⁴	5.0×10 ⁴	5.0×10 ⁴	5.0×10 ⁴	5.0×10 ⁴	5.0×10 ⁴	5.0×10 ⁴	5.0×10 ⁴	5.0×10 ⁴	5.0×10 ⁴	5.0×10 ⁴	5.0×10 ⁴	5.0×10 ⁴	5.0×10 ⁴	5.0×10 ⁴	5.0×10 ⁴	5.0×10 ⁴	5.0×10 ⁴	5.0×10 ⁴

Table 2. Birth pitch angles α , defined by equation (8), expressed in degrees at different major radial locations R , which for a 3.02 MeV proton lead to perpendicular velocities of $v_{\perp,burst} = (0.8, 0.9, 1.0, 1.1, 1.2)V_A$ at $R = 4.521$ m. It follows that these protons lie in the confined region of (α, R) parameter space delineated by the lower blue region in table 1 since the pitch angles calculated here do not exceed 35° . These pitch angle values are therefore smaller than those which lead to promptly lost ions indicated in table 1 for the range $R = 3.10$ m to $R = 4.60$ m. The box color meaning is identical to that of table 1.

R (m)	3.10	3.20	3.30	3.40	3.50	3.60	3.70	3.80	3.90	4.00	4.10	4.20	4.30	4.40	4.50	4.60
$ B (T)$	2.28	2.42	2.56	2.64	2.68	2.69	2.66	2.61	2.53	2.43	2.33	2.20	2.06	1.92	1.78	1.65
$0.8V_A$	20.29	20.94	21.56	21.91	22.08	22.13	21.98	21.78	21.42	20.99	20.52	19.91	19.23	18.55	17.83	17.14
$0.9V_A$	22.96	23.71	24.42	24.82	25.01	25.07	24.91	24.68	24.26	23.76	23.22	22.53	21.75	20.97	20.15	19.36
$1.0V_A$	25.69	26.54	27.35	27.80	28.02	28.09	27.90	27.64	27.17	26.59	25.98	25.19	24.31	23.44	22.51	21.61
$1.1V_A$	28.48	29.44	30.35	30.87	31.12	31.19	30.98	30.68	30.15	29.50	28.81	27.92	26.93	25.94	24.90	23.90
$1.2V_A$	31.34	32.42	33.45	34.04	34.32	34.40	34.16	33.83	33.22	32.49	31.72	30.72	29.60	28.51	27.35	26.23

Equating the total kinetic energy, which is the sum of perpendicular and parallel components, to the birth energy, we have:

$$\frac{1}{2}m_H v_R^2 = \frac{1}{2}m_H v_{\perp,R}^2 + \frac{1}{2}m_H v_{\parallel,R}^2 = 3.02 \text{ MeV}. \quad (7)$$

We can then compute the pitch angles α at the inferred birth locations,

$$\alpha = \arcsin\left(\frac{v_{\perp,R}}{v_R}\right), \quad (8)$$

for $v_{\perp,burst} = [0.8, 0.9, 1.0, 1.1, 1.2]V_A$ at $R = 4.521$ m. This range of values for $v_{\perp,burst}/V_A$ is chosen because it is known to give strong drive for the MCI and hence ICE [42]. Finally, we compare these values with those tabulated in table 1, to find out whether these protons are born on confined trajectories. The values of α are displayed in table 2, and suggest that the protons that intersect the burst location in the range of velocities considered were originally born on confined trajectories, as identified for LHD in table 1.

The foregoing suggests that 3.02 MeV protons with perpendicular velocities in the range $v_{\perp,burst} = [0.8-1.2]V_A$ at the location of interest are on confined trajectories. In the next section, we will show that they could efficiently drive the observed transient ICE signal. In contrast, the velocities of the energetic deuterons from perpendicular NBI are very sub-Alfvénic at the ICE location. Typically, these have $v_{\perp}/V_A < 0.3$, which has led to ICE in previous LHD experiments and modeling [14, 28], although in a different frequency range. Their ability to drive the MCI in the frequency range 250–310 MHz is weak as we show in appendix C. We need not consider them further here and focus on the larger values of v_{\perp}/V_A which are found to drive ICE more strongly in that regime.

4. Simulations of bursting ICE from LHD plasma 133979

4.1. Frequency shifts and energy partitioning

The three intense peaks *b*, *c* and *d* in figure 2 are approximately centred at frequencies 255.1, 281.7 and 308.2 MHz. In the preceding section, we used the average spacing between

these frequencies, 26.6 MHz, as an interim value for the proton cyclotron frequency Ω_H at the ICE location. If we normalise the three spectral peak frequencies to 26.6 MHz, they would correspond to proton cyclotron harmonics 9.6, 10.6 and 11.6, which are evidently not integer multiples of the fundamental. Figure 3 shows the measured power spectra in LHD plasma 133979 before the burst at $t = 4.4430$ s (top left panel) and at successive times during the burst, from $t = 4.4437$ s to $t = 4.4447$ s, in the following panels. We find that the locations of the intense spectral peaks between 250 MHz and 300 MHz in figures 2 and 3 are very close to the dashed blue lines, which correspond to $f = 26.6 \times (n + 0.6)$ MHz, $n = 8, 9, 10, 11$; they are also close to the red lines, which correspond to $f = 26.6 \times (n - 0.6)$ MHz, $n = 9, 10, 11, 12$. In a different LHD plasma, as outlined in appendix D, the peaks correspond to either $28 \times (n + 0.5)$ MHz or $28 \times (n - 0.5)$ MHz. In either case, then, the measured frequency shifts relative to integer cyclotron harmonics have magnitude $\simeq \Omega_H/2$.

Let us first examine whether, in principle, in the present context, it is plausible that there could arise Doppler shifts of 15.7 MHz (harmonics 9, 10, 11) or -10.9 MHz (harmonics 10, 11, 12). It is well known [34, 42, 51] that to excite the MCI requires the energetic ions to have perpendicular velocity $v_{\perp} \approx V_A$. The resonant condition of the n th proton cyclotron harmonic including Doppler shift is given as $\omega = k_{\parallel}v_{\parallel} + n\Omega_H$. As discussed in appendix A, both negative and positive values for $k_{\parallel}v_{\parallel}$ are possible and are captured by the simulations, and they are also observed experimentally with the subpeaks $n \pm 0.6$ in figure 3. If the total kinetic energy of the ions is sufficiently large that this value of v_{\perp} is compatible with $v_{\parallel} \simeq V_A$ also, this would provide scope for Doppler shifts satisfying $k_{\parallel}v_{\parallel} \sim \Omega_H$ if $k_{\parallel}V_A \sim \Omega_H$. This is equivalent to $(k_{\parallel}/k_{\perp})k_{\perp}V_A \sim \Omega_H$. Therefore, in the MCI, a quasi-perpendicular fast Alfvén wave is resonant with the n th proton cyclotron harmonic: $\omega_{fast} \simeq k_{\perp}V_A \simeq (n + \alpha)\Omega_H$, where α is of order 1. The MCI is typically [10] most strongly driven around the tenth proton cyclotron harmonic in deuterium plasmas, i.e. $n = 10$, see figure 1 of [34, 42] and figure 4 of [28]. For sufficiently energetic ions undergoing the MCI, the resonance condition with the inclusion of a non zero parallel velocity becomes $k_{\perp}V_A \simeq \omega = n\Omega_H \pm |k_{\parallel}v_{\parallel}|$ which suggests that it is therefore possible to satisfy $|k_{\parallel}v_{\parallel}| \sim \Omega_H$ at $\omega \sim n\Omega_H$ if $|k_{\parallel}/k_{\perp}| \sim 1/n$. It follows—but only at back-of-envelope

Table 3. The consequences of different partitions of 3.02 MeV proton energy into perpendicular and parallel components, expressed in terms of velocities normalised to the local Alfvén speed $V_A = 0.9105 \times 10^7 \text{ ms}^{-1}$ in the ICE emitting region of LHD plasma 133979 during the bursty event at $t = 4.444 \text{ s}$. The last column shows the corresponding circulation frequency due to the combined curvature and grad B guiding centre drifts, and demonstrates that this is small compared to Ω_H .

Species	v_{\perp}/V_A	Energy \perp (keV)	v_{\parallel}/V_A	Energy \parallel (keV)	ω_{Drift}/Ω_H
H	0.50	108.16	2.59	2891.84	0.0144
H	0.60	155.76	2.56	2844.24	0.0143
H	0.63	170.00	2.63	2830.00	0.0142
H	0.70	212.00	2.54	2788.00	0.0141
H	0.80	276.90	2.51	2723.10	0.0140
H	0.90	350.45	2.47	2649.55	0.0138
H	1.00	432.66	2.44	2567.34	0.0136
H	1.10	523.52	2.39	2476.48	0.0134
H	1.20	623.03	2.34	2376.97	0.0131

level—that it might be possible for a strongly non-Maxwellian population of 3.02 MeV protons to excite, through the MCI, waves at cyclotron harmonics that are Doppler shifted by the large amount $\sim \Omega_H/2$ that is observed. As an illustration, let us suppose:

$$|k_{\parallel} v_{\parallel}| \sim \Omega_H/2, \quad (9)$$

for waves excited on the fast Alfvén branch at the tenth harmonic of Ω_H , so that:

$$\omega \sim k_{\perp} V_A \sim 10\Omega_H. \quad (10)$$

Then upon taking the ratio of each side of equations (9) and (10), we find:

$$\frac{k_{\parallel}}{k_{\perp}} \sim \frac{V_A}{20u_{\parallel}} \sim \frac{1}{48.4} \quad (11)$$

for the case $u_{\parallel} = 2.42V_A$ which is inferred from equation (2) of section 1 when $u_{\perp} = 1.05V_A$. It follows that fast Alfvén waves propagating only 1° or 2° from perpendicular to \mathbf{B}_0 could in principle undergo wave-particle cyclotron harmonic resonance at the required, highly shifted, frequency of approximately $10\Omega_H \pm \Omega_H/2$. The question then is: are such waves actually excited? This motivates our direct numerical simulations reported below and in appendix B.

Table 3 displays the consequences of different partitions of the 3.02 MeV proton birth energy into perpendicular and parallel components, in terms of the corresponding perpendicular and parallel velocities normalised to the local Alfvén speed at the emission location in LHD. Guiding centre drifts enter into the MCI wave-particle resonance condition through an additional term $\mathbf{k} \cdot \mathbf{v}_{drift}$ [78]. *A priori* this will be extremely small, for reasons of vector orientation, as follows. The ICE is detected on LHD using a dipole antenna whose centre is very close to the equatorial plane, about one degree below it, and we know that MCI-excited waves have k -vectors that are quasiperpendicular to the magnetic field. In combination, these conditions imply that the detected k -vector is close to horizontal. In contrast, the curvature and $\nabla \mathbf{B} \times \mathbf{B}$ guiding centre drifts are vertical for a particle in the equatorial plane. Thus \mathbf{k} and \mathbf{v}_{drift} are perpendicular to each other, or nearly so, for the particles

and waves of interest. To check what ‘nearly so’ means, we have calculated realistic orbits for the particles of interest using the standard code for LHD. The resulting magnitude of \mathbf{v}_{drift} is an order of magnitude lower than v_{\parallel} . Hence $\mathbf{k} \cdot \mathbf{v}_{drift}$ is down by a large factor, on two counts, compared to the effects that are retained in our 1D3V slab geometry PIC computations. We shall use PIC-hybrid simulations to explore the range of k_{\parallel} which, together with v_{\parallel} , could result in frequency shifts consistent with the measured ICE power spectrum. Hitherto, no wavenumber measurements of ICE have been reported from LHD. Each PIC-hybrid computation is run at a given angle between the magnetic field \mathbf{B}_0 and the 1D spatial simulation domain, which we identify as the outward radial direction in LHD, and which defines the orientation of possible \mathbf{k} vectors.

4.2. Simulations with zero parallel velocity

As a first step in isolating the role of v_{\parallel} , we run simulations for which $u_{\parallel} = 0$, so that the initial velocity distribution function of protons is given by a ring beam $f_H = [n_{proton}/(2\pi v_{\perp})] \delta(v_{\parallel}) \delta(v_{\perp} - u_{\perp})$. The initial distribution in gyroangles is sampled randomly uniformly, and ion gyromotion is fully resolved, such that the physics of cyclotron resonant effects unfolds at the level of interactions between ions moving on their gyro-orbits and the local self-consistent electric and magnetic fields. This enables us to focus on the role of u_{\perp} . We know that $u_{\perp} \approx V_A$ is typical for the MCI to occur. With u_{\perp} in this range, and $u_{\parallel} = 0$ for now, the total kinetic energy of such protons is less than 3.02 MeV. We explore a range of perpendicular velocities from $u_{\perp} = 0.8V_A$ to $1.2V_A$. These computations use 500 particles per cell for the thermal deuterons and for the fast protons, and represent the electrons as a massless fluid. The grid has 1024 cells, and the cell size is chosen such that the cold plasma dispersion relation is recovered from the spatiotemporal Fourier transform of the electric and magnetic field fluctuations, in the appropriate limit. These provide good energy conservation, within 2% over the duration of a simulation. The time evolution of the fields and of the ion species energy density from our PIC-hybrid simulations show that the collective relaxation of the proton population with energy in the MeV range is governed by the MCI, as seen in figure 12. It is known that the MCI drive

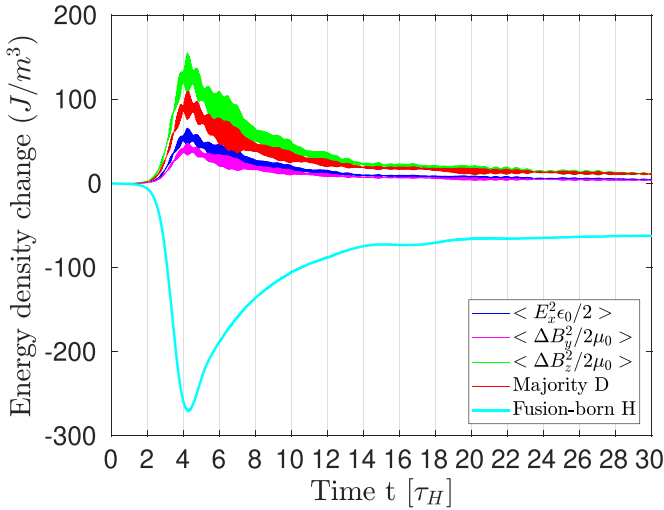


Figure 12. Time evolution of the change in energy density of the fields and of the thermal deuterons and fusion-born proton population. The latter collectively relaxes under the MCI, giving up energy to excite the electric and magnetic fields, causing the thermal deuterons to oscillate self-consistently. The magenta and green traces correspond to the y and z -components of the magnetic field. The blue and red curves show the energy density change of the x -component of the electric field and of the thermal deuterons respectively. The propagation angle between the simulation domain and the background magnetic field \mathbf{B}_0 is 91° , $u_\perp = 1.0V_A$. The time is normalised to the proton gyroperiod τ_H .

increases with the relative number density $\xi = n_{proton}/n_e$ in the relevant regime [35, 46]. In the simulations described below, the value of ξ is chosen to saturate the MCI within $20\tau_D$: $\xi = 0.0025$ for orientation of the spatial domain with respect to \mathbf{B}_0 of 90.5° , 91.0° and 91.5° ; and $\xi = 0.0050$ for 92.0° . This approach optimises the use of computational resources (each simulation requires two hours on 56 cores) without compromising the physics.

The resulting power spectra shown in figure 13 are for a range of values of the perpendicular component of velocity $0.8 \leq u_\perp/V_A \leq 1.2$. The spectral peaks are at successive proton cyclotron harmonics, and in this respect they differ, as expected, from the LHD ICE observations in figure 2 that we seek to explain. These preliminary simulation results are encouraging in relation to the essential feature of the ICE spectrum in figure 2, measured during the LHD transient, in that the simulated spectra are dominated by a few cyclotron harmonic peaks in the frequency range between $\omega = 8\Omega_H$ and $12\Omega_H$.

The magnitude of the most strongly driven spectral peaks in figure 13 tends to decrease monotonically as u_\perp increases, and this feature is most notable when the propagation angle gets closer to 90° . Figure 14 shows the sensitivity of the spectral peak maxima to the propagation angle, as well as to the perpendicular beam velocity in the range $0.925 \leq u_\perp/V_A \leq 1.050$, using higher resolution computational parameters for these simulations, as anticipated from section 4.3, namely 2000 particles per cell and 8192 cells. It confirms that, in these initial computations for the restricted case $u_\parallel = 0$, the MCI of a ring-beam population of energetic protons with $u_\perp \sim V_A$ generates simulated ICE spectra whose dominant peaks

are in the observationally significant range between $9\Omega_H$ and $12\Omega_H$. We have found that this spectral range is also dominant for an initial fast proton distribution which incorporates perpendicular thermal spread [59] $f_H \propto \exp\left[-(v_\perp - u_\perp)^2/v_{\perp,r}^2\right]$ with $v_{\perp,r} = 0.15u_\perp$. Proton cyclotron harmonics are therefore strongly driven in the range between $9\Omega_H$ and $12\Omega_H$ comparatively to other cyclotron harmonics. Cyclotron harmonics below $9\Omega_H$ tend to be more strongly excited as the ratio v_\perp/V_A further increases however our focus on the frequency range $9\Omega_H$ and $12\Omega_H$ is based on the experimental observations.

4.3. Simulations with realistic parallel velocity

The simulation results obtained in the preceding section 4.2, for the case where the driving proton population has no velocity component parallel to the magnetic field, indicate that the range of angles and u_\perp/V_A values considered give rise to robust, and potentially experimentally relevant, MCI-driven power spectra. Let us now focus in particular on $u_\perp/V_A = 1.05$, and introduce parallel velocities into our approach. For fusion-born protons, the initial kinetic energy $E = m_H(u_\perp^2 + u_\parallel^2)/2 = 3.02$ MeV. It follows from equation (2) that if $u_\perp = 1.05V_A$, then $u_\parallel = 2.42V_A$ for a 3.02 MeV proton. In the series of PIC-hybrid computations described in this sub-section, we use these values for u_\perp and u_\parallel (together with other pairings derived in the same way; see table 3) as parameters in the simple model distribution function of the fusion-born protons. Following equation (1), this is:

$$f_H(v_\perp, v_\parallel) = \frac{n_H}{2\pi v_\perp} \delta(v_\parallel - u_\parallel) \delta(v_\perp - u_\perp). \quad (12)$$

As previously, the initial distribution of proton is uniformly distributed in gyro-angles. We have run PIC-hybrid simulations for minority 3.02 MeV proton populations, initialised using equation (12), in majority thermal deuterium plasmas. We use 2000 particles per cell for each ion species, with 8192 cells, and a duration of $15\tau_H$ with a relative proton density $\xi = 0.001$ in all of the following simulations. Relative energy does not change by more than 0.5%. Power spectra are constructed from the spatiotemporal Fourier transform of δB_z , taken over the full spatial domain and averaged over $15\tau_H$. This is shown on the right panel of figure 15, where the fast Alfvén branch and multiple cyclotron harmonic wave branches are clearly visible. Summing the Fourier transformed power between $k = 0$ and $k = 24\Omega_H/V_A$ yields the power spectrum shown on the left panel in figure 15. This is identical to the green trace shown in figure 16(left). Figure 16 shows the power spectra of waves propagating in the $+\hat{x}$ direction (corresponding to the direction of the 1D simulation domain) at an angle of 91.0° and 90.8° with respect to the background magnetic field \mathbf{B}_0 . The green power spectra result from 3.02 MeV protons whose parallel and perpendicular velocities are $u_\parallel = 2.415V_A = 2.199 \times 10^7$ ms $^{-1}$ and $u_\perp = 1.050V_A = 0.956 \times 10^7$ ms $^{-1}$; while the blue traces have the same value of u_\perp but with $u_\parallel = 0$, for comparison (as in section 4.2). The frequency resolution in the computed spectra is $\pm 0.07\Omega_H$. In the blue cases, for zero u_\parallel , three intense spectral peaks appear

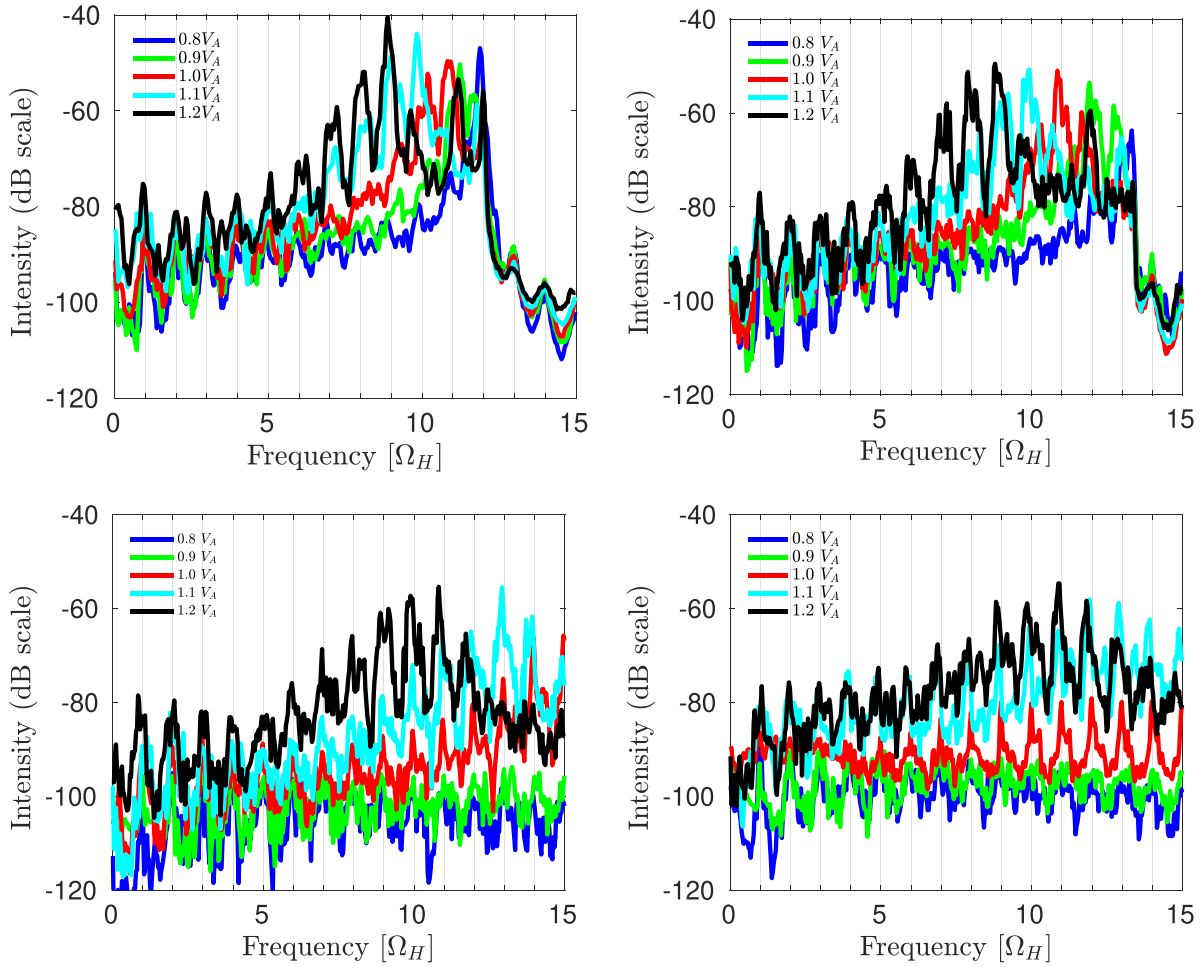


Figure 13. Power spectra of the excited δB_z energy density in multiple computations of the relaxation of a ring-beam ($u_{\parallel} = 0$) distribution of protons for LHD plasma 133979 parameters at the time and location of the bursting ICE event. For the five spectra plotted in each panel, the protons have purely perpendicular velocity u_{\perp} : from top, $u_{\perp} = 1.2 V_A$, $1.1 V_A$, $1.0 V_A$, $0.9 V_A$ and $0.8 V_A$. The propagation angle between \mathbf{k} and \mathbf{B}_0 is 90.5° (top left), 91.0° (top right), 91.5° (bottom left), 92.0° (bottom right).

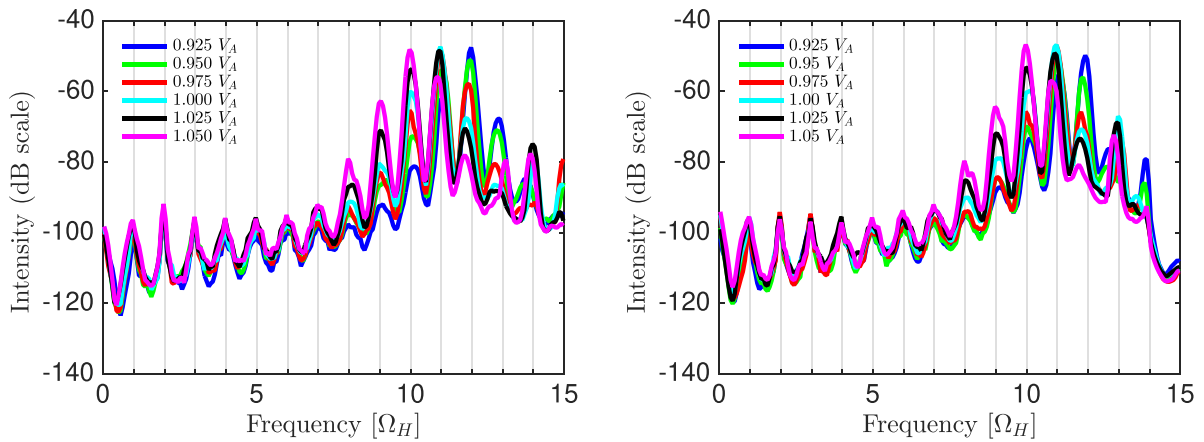


Figure 14. Power spectra for oscillations excited by a ring-beam ($v_{\parallel} = 0$) proton population at a propagation angle of 91.0° (left), and 90.8° (right), for different perpendicular beam velocities (inset), in the range $0.925 \leq u_{\perp}/V_A \leq 1.050$. In both cases, the four dominant spectral peaks that result from the simulations are the ninth to twelfth harmonics of Ω_H . These correspond exactly to the four cyclotron harmonics of greatest relevance to the interpretation of the measured ICE spectral peaks *b*, *c* and *d* in figure 2.

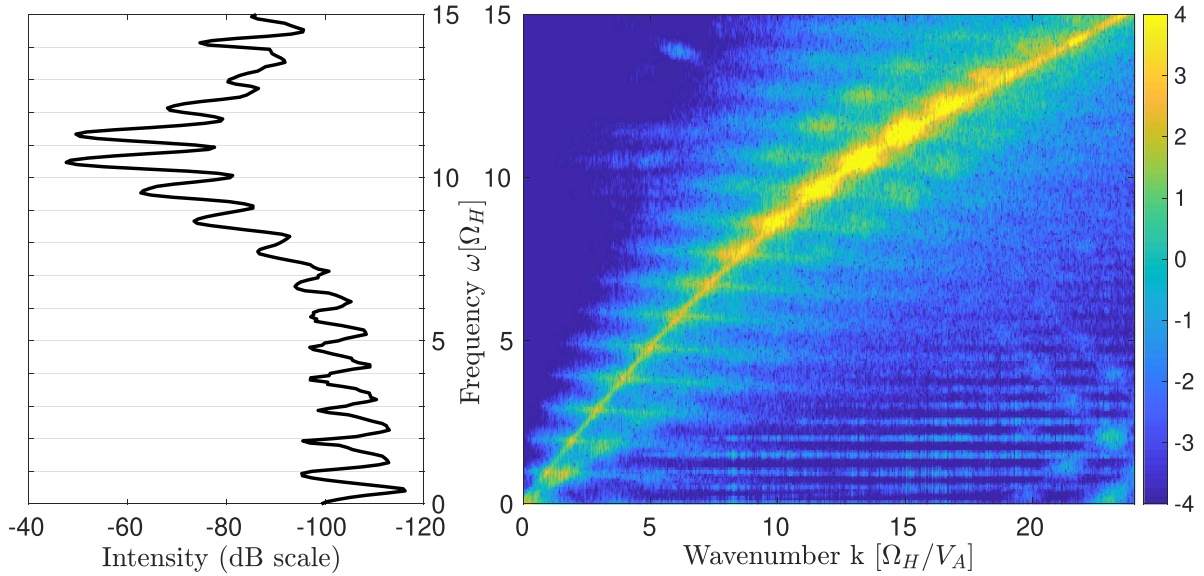


Figure 15. The power spectrum of δB_z (left) is constructed from the spatiotemporal Fourier transform of δB_z (right). These are plotted on a dB and \log_{10} scale respectively, for the fields excited by the relaxation of a 3.02 MeV proton population initialised with $[n_H/(2\pi v_\perp)]\delta(v_\parallel - u_\parallel)\delta(v_\perp - u_\perp)$, $u_\perp = 1.05V_A$ and $u_\parallel = 2.42V_A$. The propagation angle between \mathbf{k} and \mathbf{B}_0 is 91.0° , and the majority thermal ions are deuterons.

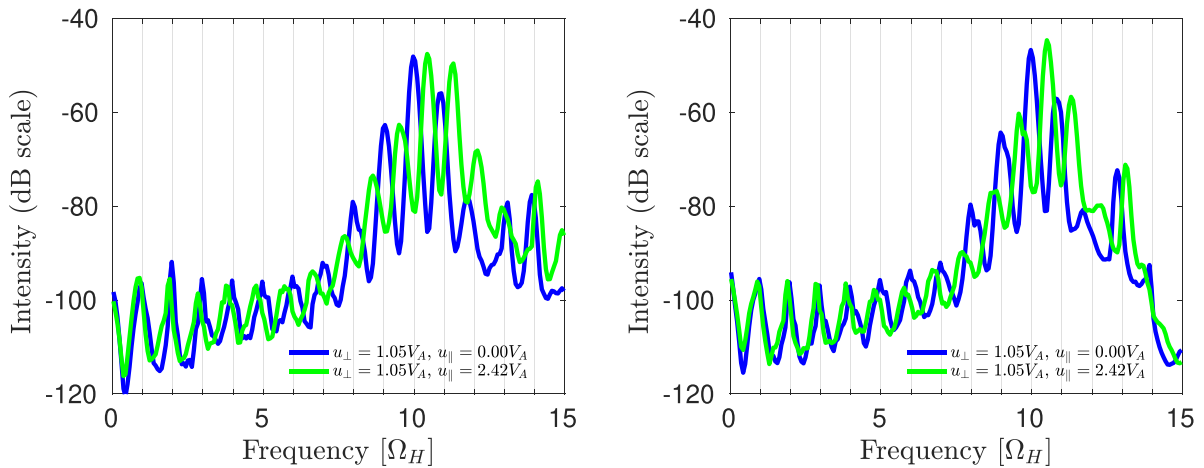


Figure 16. Power spectra of δB_z from PIC-hybrid computations with the orientation of the spatial domain $\hat{\mathbf{x}}$ at an angle of 91.0° (left) and 90.8° (right) with respect to the background magnetic field. Only excited waves propagating in the $+\hat{\mathbf{x}}$ direction are included. The initial energetic proton distribution functions are $[n_H/(2\pi v_\perp)]\delta(v_\parallel)\delta(v_\perp - u_\perp)$ (blue trace) and $[n_H/(2\pi v_\perp)]\delta(v_\parallel - u_\parallel)\delta(v_\perp - u_\perp)$ (green trace). The velocities are $u_\parallel = 2.199 \times 10^7 \text{ ms}^{-1}$ and $u_\perp = 0.956 \times 10^7 \text{ ms}^{-1}$, corresponding to $u_\perp = 1.05V_A$ and $u_\parallel = 2.42V_A$ and are such that $m_H(u_\parallel^2 + u_\perp^2)/2 = 3.02 \text{ MeV}$. The dominant spectral peaks for the green traces are at: (left) $9.50\Omega_H$, $10.44\Omega_H$ and $11.30\Omega_H$; (right) $9.57\Omega_H$, $10.50\Omega_H$ and $11.30\Omega_H$.

at $9\Omega_H$, $10\Omega_H$ and $11\Omega_H$. For the green traces in figure 16, with $u_\parallel = 2.42V_A$, the dominant spectral peaks are at: $9.50\Omega_H$, $10.44\Omega_H$ and $11.30\Omega_H$ for 91.0° propagation angle; and at $9.57\Omega_H$, $10.50\Omega_H$ and $11.30\Omega_H$ for 90.8° . We note immediately that the spectral peak frequencies are shifted by approximately $\Omega_H/2$, similar to the observational shifts noted at the start of section 4.1.

For a second set of simulations using protons initialised with $u_\perp = 0.950V_A = 0.865 \times 10^7 \text{ ms}^{-1}$ and $u_\parallel = 2.470V_A = 2.244 \times 10^7 \text{ ms}^{-1}$, at a propagation angle of 89.0° , the

MCI-excited spectrum is shown in figure 17. This has major peaks at $9.49\Omega_H$, $10.57\Omega_H$ and $11.57\Omega_H$.

As noted at the start of section 4.1, the observed frequencies of the ICE spectral peaks *b*, *c* and *d* in figure 2 could be provisionally identified with $9.6\Omega_H$, $10.6\Omega_H$ and $11.6\Omega_H$. The extent of agreement between these experimental values and the results of first principles simulation embodied in the green spectra of figures 16 and 17 appears encouraging. The four dominant spectral peaks as a function of (u_\perp, u_\parallel) are given in tables 4 and 5 for waves propagating in the $+\hat{\mathbf{x}}$ direction of the

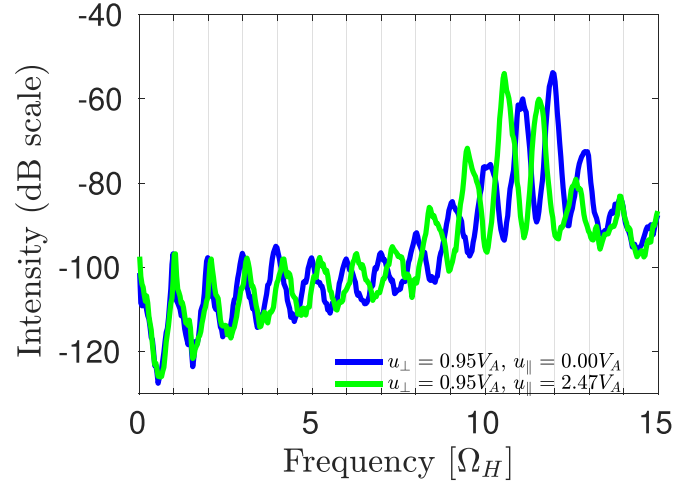


Figure 17. Power spectrum of δB_z from a PIC-hybrid computation for waves excited propagating in the $+\hat{x}$ direction, which is oriented at an angle of 89.0° with respect to the background magnetic field. The initial energetic proton distribution functions have the form defined in the caption to figure 16, with $u_\perp = 0.95V_A$ and $u_\parallel = 2.47V_A$. The dominant spectral peaks for the green traces are at $9.49\Omega_H$, $10.57\Omega_H$ and $11.57\Omega_H$.

Table 4. Location of the four major peaks in the simulated ICE spectrum, in units of Ω_H , for drifting ring-beam populations of minority 3.02 MeV protons initialised with five different combinations of (u_\perp, u_\parallel) as shown. In all cases the waves are forward propagating, and the propagation angle between the simulation domain and the background magnetic field \mathbf{B}_0 is 91.0° . The frequency resolution in the computed spectra is $\pm 0.07\Omega_H$.

$u_\perp, u_\parallel (V_A)$ \ ℓ	9	10	11	12	13	14	15
$u_\perp = 0.90, u_\parallel = 2.48$	—	—	—	11.37	12.30	13.10	13.97
$u_\perp = 0.95, u_\parallel = 2.47$	—	—	10.44	11.37	12.24	13.04	—
$u_\perp = 1.00, u_\parallel = 2.44$	—	9.57	10.44	11.30	12.17	—	—
$u_\perp = 1.05, u_\parallel = 2.42$	—	9.50	10.44	11.30	12.10	—	—
$u_\perp = 1.10, u_\parallel = 2.39$	8.70	9.57	10.37	11.17	—	—	—

Table 5. The same as table 4 for a propagation angle of 89° .

$u_\perp, u_\parallel (V_A)$ \ ℓ	7	8	9	10	11	12	13
$u_\perp = 0.90, u_\parallel = 2.48$	—	—	—	10.57	11.64	12.64	13.7
$u_\perp = 0.95, u_\parallel = 2.47$	—	—	9.50	10.57	11.57	12.57	—
$u_\perp = 1.00, u_\parallel = 2.44$	—	8.44	9.50	10.50	11.50	—	—
$u_\perp = 1.05, u_\parallel = 2.42$	7.30	8.37	9.44	10.37	—	—	—
$u_\perp = 1.10, u_\parallel = 2.39$	7.30	8.37	9.44	10.37	—	—	—

simulation domain, at angles of 91.0° and 89.0° with respect to the background magnetic field \mathbf{B}_0 .

There is a further interesting aspect to the simulated power spectra shown by green traces in figures 16 and 17, which correspond to simulations with super-Alfvénic u_\parallel : the peaks at lower frequencies lie very close to low integer cyclotron harmonics. This is in contrast to the substantial frequency shifts that are visible at higher harmonics, and are tabulated in tables 4 and 5.

We have performed additional simulations spanning a range of parallel velocities in $v_\parallel/V_A = [0.0 : 0.1 : 2.6]$ at fixed v_\perp showing that the resonance position varies smoothly with v_\parallel and achieves significant spectral shifts for $v_\parallel \sim V_A$ and observed the same behaviour when repeating the process with a different value of v_\perp/V_A .

5. Conclusions

The transient ICE spectrum from LHD plasma 133979, and in particular peaks *b*, *c* and *d* of figure 2, present an interesting and potentially important challenge to the understanding of energetic ion physics in this LHD heliotron-stellarator plasma, and more widely. While the frequency separation of successive peaks can be identified with the proton cyclotron frequency Ω_H at a specific radial location in the outer edge plasma, the peak frequencies cannot be identified with integer multiples of Ω_H : instead they are closer to integer-plus-one-half values. There are two energetic proton populations that are present in this deuterium plasma, with velocity-space inversions which could potentially enable them to drive the MCI and hence ICE. These are NBI-injected ions, and fusion-born protons which

are created at 3.02 MeV. Careful analysis, see table 1, shows that a distinct velocity-space subset of the fusion-born protons is confined, as distinct from being promptly lost, depending on pitch angle at birth in the spatial location of interest. In this paper, we have shown that this proton population is capable of driving the ICE signal, and is a more likely source than the NBI ions.

We have carried out multiple PIC-hybrid computations of the collisionless relaxation of a freshly fusion-born proton population at 3.02 MeV, with a restricted range of pitch angles reflecting table 1, within a majority thermal deuterium plasma with parameters appropriate to LHD plasma 133979. The computations follow first-principles full ion-gyro-orbit self-consistent Maxwell–Lorentz physics for very large numbers of particles. Taken together, the phenomenology of particles and fields is consistent with the analytical theory of the MCI. The power spectrum constructed from the temporal Fourier transform of the excited fields, in the saturated regime of the instability, constitutes our simulated ICE spectrum.

All our simulated ICE spectra show dominant spectral peaks separated approximately by the proton cyclotron frequency Ω_H evaluated at $R = 4.234$ m, in the frequency range between $8\Omega_H$ and $12\Omega_H$, see section 4. We find good mappings from the simulated ICE spectra to the three intense peaks from the measured LHD spectrum in figure 2, provided that the protons are initialised with $v_{\parallel} = 2.5V_A$, consistent with $v_{\perp} \sim V_A$ and $E_H = 3.02$ MeV. The excited waves propagate almost perpendicular to the background magnetic field, that is, radially out of the plasma. The simulated results have been obtained using a simple drifting ring distribution for the protons in velocity-space, and additional simulations show that the inclusion of thermal spread in the ring only slightly affects the relative strength of the most intense harmonics. The propagation angle also affects the calculated spectra. Having noted these relatively minor sensitivities, the underlying conclusion appears robust: the measured ICE spectrum from LHD deuterium plasma 133979 shown in figure 2 is probably excited by the fast relaxation of a transient local population of fusion-born protons at 3.02 MeV whose perpendicular velocity is close to the Alfvén speed, and whose parallel velocity is therefore ~ 2.5 times higher. We believe this may be the first observation of collective radiation from a confined population of fusion born-ions to be reported from a heliotron-stellarator plasma. Disambiguation between two or more energetic ion species that could potentially generate complex observed ICE spectra is an increasing challenge, and the results and methodology developed here will assist this. Our approach is also expected to be relevant to ICE driven by ion beams with lower parallel velocities, for example in cylindrical plasma experiments.

This first probable detection of collective electromagnetic radiation from fusion-born ions in a stellarator-type plasma is an encouraging development for MCF plasma physics, and shows the flexibility of the LHD heliotron-stellarator and its diagnostic systems. This result also demonstrates the role of ion cyclotron emission as a particularly sensitive diagnostic for fusion-born ion populations. Here on LHD, as previously

in JET, TFTR and KSTAR [9, 10, 24, 41], ICE has been detected from a quasi-trace subset of the fusion-born ion population with distinctive properties in velocity-space, whose presence was unsuspected until their ICE was detected and then interpreted. Arguably this sensitivity reinforces the case for the adoption of ICE as a fast ion diagnostic in ITER.

Data availability statement

The data that support the findings of this study are available upon reasonable request from the authors.

Acknowledgments

This work has been carried out within the framework of the EUROfusion Consortium and has received funding from the Euratom research and training programme 2014–2018 and 2019–2020 under Grant Agreement No. 633053. The work received support from the RCUK Energy Programme (Grant No. EP/T012250/1), NIFS budget NIFS15KLPF045 and from NRF Korea Grant No. 2014M1A7A1A03029881. The views and opinions expressed herein do not necessarily reflect those of the European Commission. R O D acknowledges the hospitality of Kyushu University. B C G R acknowledges helpful discussions with Prof. Mark Koepke, Dr Kenneth G McClements and with Dr Leopoldo Carbajal-Gomez. The authors are grateful to both referees for their painstaking and constructive questions and commentary on the initially submitted version of this manuscript.

Appendix A. Positive and negative frequency shifts

In evaluating the frequency shifts, we are interested in the values taken by $\omega - k_{\parallel}v_{\parallel}$ and particularly in the sign of the term $k_{\parallel}v_{\parallel}$. This sign depends on the respective orientations of \mathbf{v} and of \mathbf{k} . In the simulations, v_{\parallel} is an input which is always set positive, but could also be negative, while positive and negative values of k_{\parallel} both coexist in the simulations; this enables coverage of both possible signs of the frequency shift. In other words, for a fixed sign of v_{\parallel} , co- and counter-propagating waves will result in opposite signs of k_{\parallel} . If instead, the direction of k_{\parallel} is set, fusion-born ions with either $v_{\parallel} > 0$ or $v_{\parallel} < 0$ could account for the sign. Typically, PIC simulations for ICE have $\mathbf{B}_0 = B_0\hat{\mathbf{z}}$, that is \mathbf{B}_0 is perpendicular to the one-dimensional spatial simulation domain, whose direction is denoted by $\hat{\mathbf{x}}$. In our current work, \mathbf{B}_0 is almost perpendicular to the x -axis. If the angle between \mathbf{B}_0 and $\hat{\mathbf{x}}$ is let us say 89.0 degrees, the projection $B_{0,x}$ of \mathbf{B}_0 on the x -axis is positive, whereas if this angle is 91 degrees, then $B_{0,x}$ is negative. The foregoing are the combinations of the parameters $(\mathbf{B}_0, \pm\|\mathbf{k}\|, \pm v_{\parallel})$ which eventually determine the sign of $k_{\parallel}v_{\parallel}$. There are symmetries, in that changing the angle between the background magnetic field and the x -axis from $(90 - \alpha)$ degrees to $(90 + \alpha)$ degrees, and changing the sign of \mathbf{k} at the same time yield the same

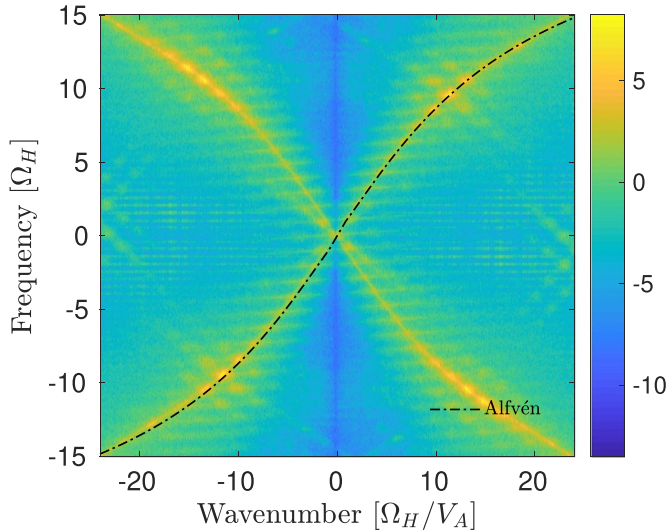


Figure 18. Spatiotemporal Fourier transform of the fluctuating part of δB_z . The angle between $\hat{\mathbf{x}}$ and \mathbf{B}_0 is 91° . The physical quantities are real numbers and this implies that the top right and bottom left quadrants are identical, as are the top left and bottom right quadrants. This is because real signals $\cos(\omega t \pm kx) = 1/2(\exp(i(\omega t \pm kx)) + \exp(-i(\omega t \pm kx)))$ contain both positive and negative frequencies of equal amplitudes. When ω and k have the same sign, the waves propagate backward, these correspond to waves that lie in the top right and bottom left quadrants. Conversely, if ω and k have opposite signs, the waves propagate forward, these correspond to waves that lie in the top left and bottom right quadrants.

power spectra. As a corollary, the power spectra summed over both positive and negative values of the wavevector along the simulation direction $\hat{\mathbf{x}}$ ($\mathbf{k} \cdot \hat{\mathbf{x}} \leq 0$) are identical in these two cases. The Fourier transform decomposes our simulated signals in the form of $A(\omega, \mathbf{k}) \exp(+i(\omega t + \mathbf{k} \cdot \mathbf{x})) = A(\omega, k) \exp(+i(\omega t + kx))$, k the component along $\hat{\mathbf{x}}$. The amplitude of the modes $A(\omega, k)$ are shown in figure 18 and zoomed in figure 19. The phase $\omega t + kx$ corresponds to waves propagating forward, in the $+\hat{\mathbf{x}}$ direction when $k < 0$ and backward in the $-\hat{\mathbf{x}}$ direction when $k > 0$. By convention, the power spectra are calculated by considering $\omega > 0$ in figure 18 and summed over the relevant range of k -values as shown in figures 20 and 21.

We provide two possible explanations for the unequal frequency spacing in these power spectra. The first relates to the frequency resolution which depends on the length of the time series. The Nyquist criterion implies that the maximum frequency captured in our calculations corresponds to $\nu_{max} = 1/2\Delta t$ with Δt the time step of the simulation chosen to be $5 \times 10^{-4}\tau_H$, with τ_H the proton gyroperiod. The time step for saving the numerical outputs used for the Fourier transforms is $\Delta t = 5 \times 10^{-3}\tau_H$. Thus $\nu_{max} = 1/(2 \times 5 \times 10^{-3} \times \tau_H) = 100/\tau_H$ and therefore $\omega_{max}/\Omega_H = 100$. Conversely, the frequency spacing $\Delta\omega$ is given by $2\pi/T$, with T the duration of the simulation and taken to be $T = 15 \times \tau_H$, which leads to $\Delta\omega = 2\pi/(15 \times \tau_H) = \Omega_H/15 = 0.07\Omega_H$. This value is introduced in the caption of table 4

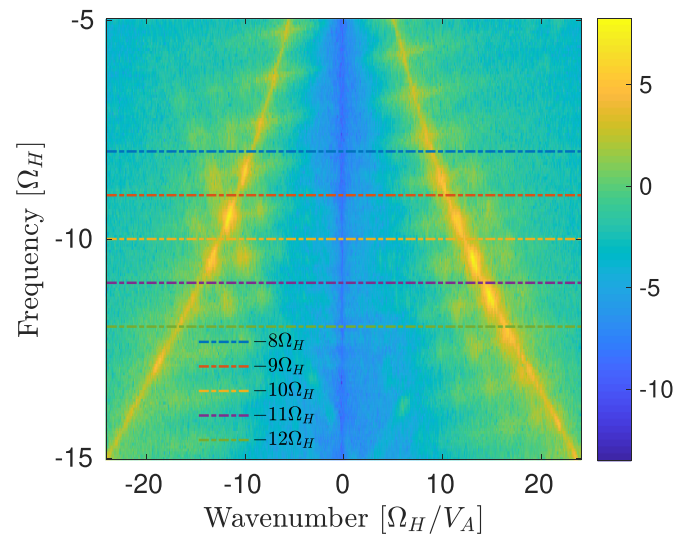
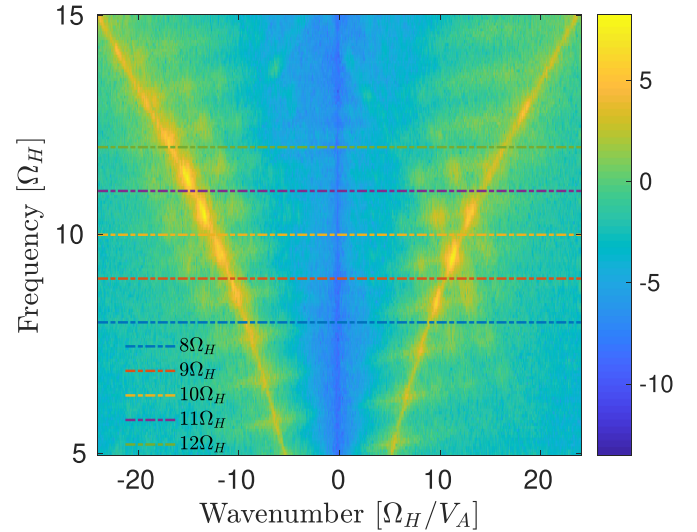


Figure 19. The proton cyclotron harmonics zoomed from figure 18 are shifted differently depending on the sign of the wavenumber k . The right (left) zone in the top the panel is symmetric to the left (right) area in the bottom panel.

and can partially explain the different frequency spacings of $0.87\text{--}0.94\Omega_H$ and $0.92\text{--}1.07\Omega_H$. We have also performed simulations over $60\tau_H$ to increase the resolution in frequency space to $\Delta\omega = 0.017\Omega_H$ and observe the same phenomenology: the spectral peaks spacing is not exactly constant. Non-linear beating between cyclotron harmonics could give rise to additional excitations. This mechanism has been successfully tested in previous works, see for example figure 6 of [34] and additional nonlinear wave analysis in figure 4 of [28]. This phenomenon could give us a hint as to why the frequency spacing appears uneven: low cyclotron harmonics are linearly stable and grow due to the beating between high-harmonics-spectrally-shifted cyclotron waves. The spectral shift of the linearly stable cyclotron harmonics ω_1 , driven non linearly, would result from the sum (or difference) of the high frequency, linearly unstable, waves ω_2 and ω_3 , namely

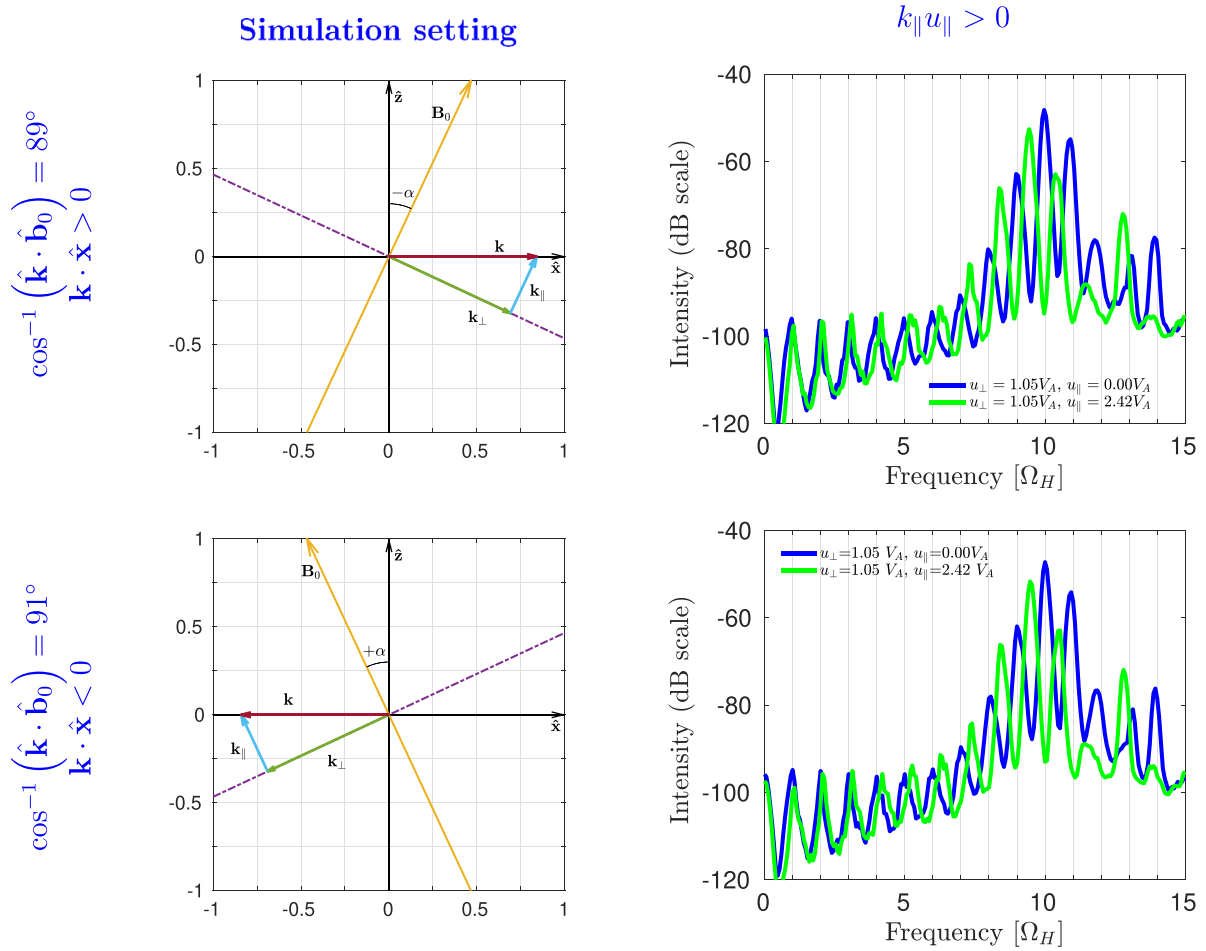


Figure 20. Geometry setting (left panels) and power spectra of δB_z (right panels) from PIC-hybrid computations with the orientation of the background magnetic field at an angle of 89.0° (top panels) and 91.0° (bottom panels) with respect to the spatial domain $+\hat{\mathbf{x}}$. The initial value of u_{\parallel} is strictly positive. Excited waves propagating in both the $+\hat{\mathbf{x}}$ direction (spectrum summed over $k > 0$, see figure 18; top panels) and in the $-\hat{\mathbf{x}}$ direction (spectrum summed over $k < 0$, see figure 18; bottom panels) result in the same power spectra when changing the angle from $-\alpha$ to $+\alpha$ between the vectors $\hat{\mathbf{z}}$ and \mathbf{B}_0 . Proton cyclotron harmonics are shifted to the left since $k_{\parallel} u_{\parallel} > 0$. The initial energetic proton distribution functions are $[n_H/(2\pi v_{\perp})] \delta(v_{\parallel}) \delta(v_{\perp} - u_{\perp})$ (blue trace) and $[n_H/(2\pi v_{\perp})] \delta(v_{\parallel} - u_{\parallel}) \delta(v_{\perp} - u_{\perp})$ (green trace). The magnitude of the background magnetic field is 1.75 T. The velocities are $u_{\parallel} = 2.199 \times 10^7 \text{ ms}^{-1}$ and $u_{\perp} = 0.956 \times 10^7 \text{ ms}^{-1}$, corresponding to $u_{\parallel} = 2.42 V_A$ and $u_{\perp} = 1.05 V_A$ and are such that $m_H(u_{\parallel}^2 + u_{\perp}^2)/2 = 3.02 \text{ MeV}$.

$\omega_3 = \omega_1 + \omega_2$. Therefore the spectral shift of ω_3 would be the sum of the spectral shifts of ω_1 and ω_2 and explain the uneven frequency spacing. In particular, as shown in the power spectra of figure 22, which correspond to the bottom right panels of figures 20 and 21, the fundamental cyclotron frequencies are slightly offset. On the left panel, the first peak of the green trace locates between 0.86 and $0.90 \Omega_H$ and the most intense peaks are located at 9.503 , 10.440 and $11.300 \Omega_H$. The successive differences give $10.440 - 9.503 = 0.940$ and $11.300 - 10.440 = 0.860$. On the right panel, the first peak of the green trace is located at $1.034 \Omega_H$ and the strongest peaks are at 8.369 , 9.436 and $10.370 \Omega_H$. The successive differences yield $10.370 - 9.436 = 0.9340$ and $9.436 - 8.369 = 1.0670$. Therefore the differences between the three successive intense peaks correspond roughly to the down-shifted and up-shifted fundamental proton cyclotron frequencies which coexist in the simulations. These suggest the presence of nonlinear wave

interactions and are related to the faint spots away from the linear fast-Alfvén wave branch in the dispersion relation graph of figure 18.

Appendix B. Simulation at 85° , higher k_{\parallel}

We have shown in section 4.1 that strong shifts can be achieved for angles as low as 1° or 2° from perpendicular to \mathbf{B}_0 . Strong shifts can in principle also be achieved at small v_{\parallel} with high k_{\parallel} . We have run a hybrid-PIC simulation at 85° which leads to higher values of k_{\parallel} compared to those run at 89° . The thermal electron and deuterium temperatures are 846 eV and 907 eV respectively, while the electron number density is $8.8 \times 10^{18} \text{ m}^{-3}$ and $B_0 = 1.75 \text{ T}$ such that $V_A = 0.9105 \times 10^7 \text{ ms}^{-1}$ as per section 3. The power spectrum corresponding to a propagation angle of 85° (89°) in figure 23 is obtained using 4000 (2000) macroparticles per

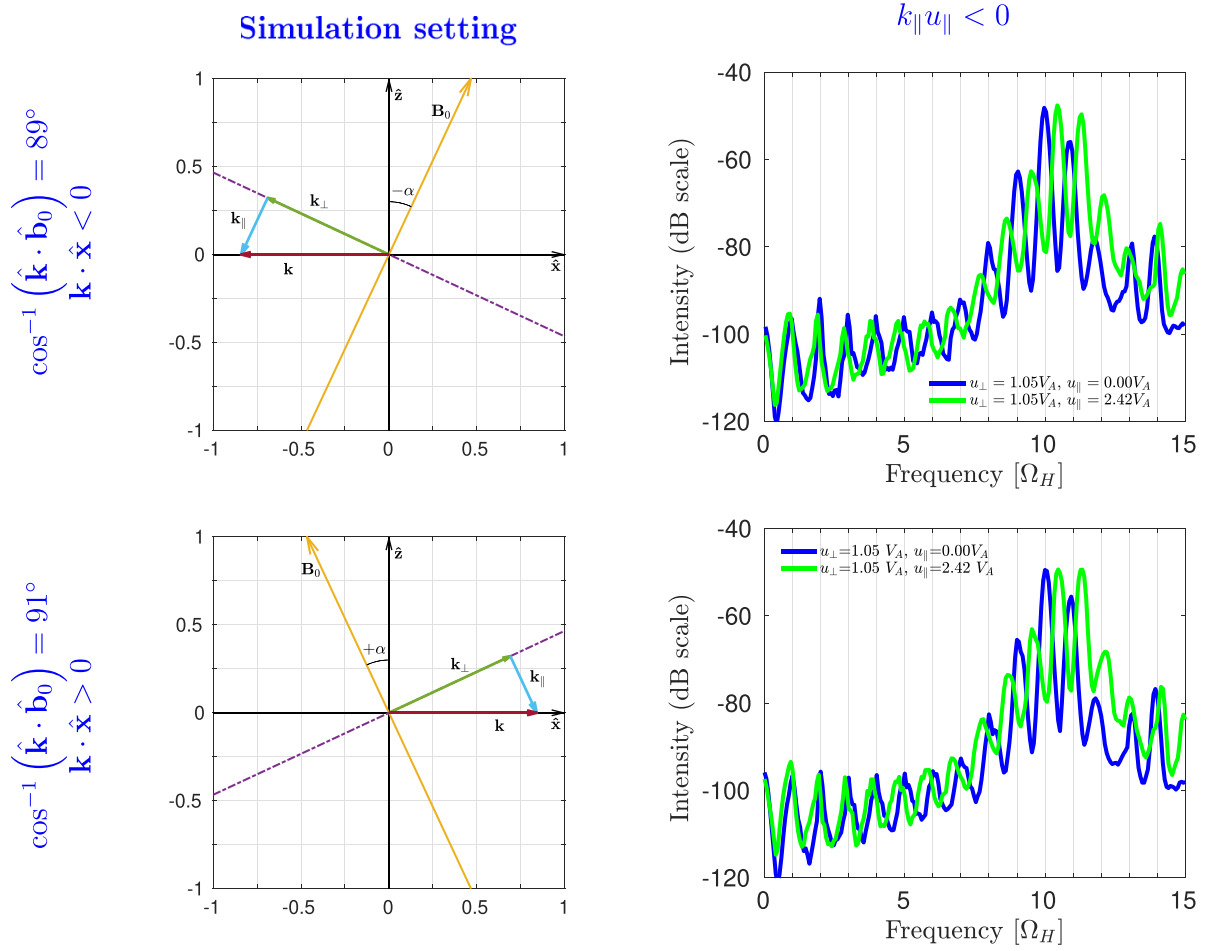


Figure 21. Geometry setting (left panels) and power spectra of δB_z (right panels) from PIC-hybrid computations with the orientation of the background magnetic field at an angle of 89.0° (top panels) and 91.0° (bottom panels) with respect to the spatial domain $\hat{\mathbf{x}}$. The initial value of u_{\parallel} is strictly positive. Excited waves propagating in both the $-\hat{\mathbf{x}}$ direction (spectrum summed over $k < 0$; top panels) and in the $+\hat{\mathbf{x}}$ direction (spectrum summed over $k > 0$; bottom panels) result in the same power spectra when changing the angle from $-\alpha$ to $+\alpha$ between the vectors $\hat{\mathbf{z}}$ and \mathbf{B}_0 . Proton cyclotron harmonics are shifted to the right since $k_{\parallel} u_{\parallel} < 0$. The initial energetic proton distribution functions are $[n_H/(2\pi v_{\perp})] \delta(v_{\parallel}) \delta(v_{\perp} - u_{\perp})$ (blue trace) and $[n_H/(2\pi v_{\perp})] \delta(v_{\parallel} - u_{\parallel}) \delta(v_{\perp} - u_{\perp})$ (green trace). The magnitude of the background magnetic field is 1.75 T. The velocities are $u_{\parallel} = 2.199 \times 10^7 \text{ ms}^{-1}$ and $u_{\perp} = 0.956 \times 10^7 \text{ ms}^{-1}$, corresponding to $u_{\parallel} = 2.42 V_A$ and $u_{\perp} = 1.05 V_A$ and are such that $m_H(u_{\parallel}^2 + u_{\perp}^2)/2 = 3.02 \text{ MeV}$.

cell, with 4096 (8192) grid cells and a relative fusion born-proton density $\xi = 0.001$ (0.005) and calculated over $15\tau_H$ ($35\tau_H$). The instability unfolds more slowly at 85° and is the reason for using a higher ξ -value [14]. These power spectra further stress the asymmetry between spectral peaks obtained either with $k > 0$ or $k < 0$, the asymmetry being both in peak location and peak amplitude. We also note that the most intense peaks at 85° are obtained at lower cyclotron harmonics (1–6) while at 89° , they appear at higher cyclotron harmonics (8–12). This follows the trend of figure 13 suggesting that ICE is less strongly driven between the 8th–12th proton cyclotron harmonics when the propagation angle departs from perpendicular. Although other pairs of $(k_{\parallel}, k_{\perp})$ and $(v_{\parallel}, v_{\perp})$ are possible for significant spectral shift, we have focused on quasi-perpendicular propagating waves as these simultaneously show excitations in the range 8th to 12th proton cyclotron harmonics and generate substantial frequency shifts when they are driven by fusion-born protons.

Appendix C. 69 keV \perp D-NBI and 170 keV \parallel H-NBI

The plasma studied in the present work was heated by 69 keV perpendicular NBI deuterons and 170 keV parallel NBI protons. We have therefore tested the hypothesis that 69 keV NBI deuterons drive ICE by carrying a simulation using the plasma parameters reported in the manuscript (thermal electron and deuteron temperatures $T_e = 846 \text{ eV}$ and $T_D = 907 \text{ eV}$ respectively, $n_e = 8.8 \times 10^{18} \text{ m}^{-3}$ and $B_0 = 1.75 \text{ T}$). The simulation grid consisted of 8192 cells, each initially loaded with 2000 thermal deuterons per cell and 2000 NBI deuterons per cell. These 69 keV NBI deuterons are initialised in velocity space with a ring-beam distribution $\propto \delta(v_{\parallel}) \delta(v_{\perp} - u_{NBI})$ and the relative density is chosen to be $n_{DNBI}/n_e = 0.020$. The angle between the background magnetic field and the simulation domain is set to 91° . The power spectrum appearing on the right panel of figure 24, which is normalised to the proton cyclotron frequency, suggests that ICE is excited in

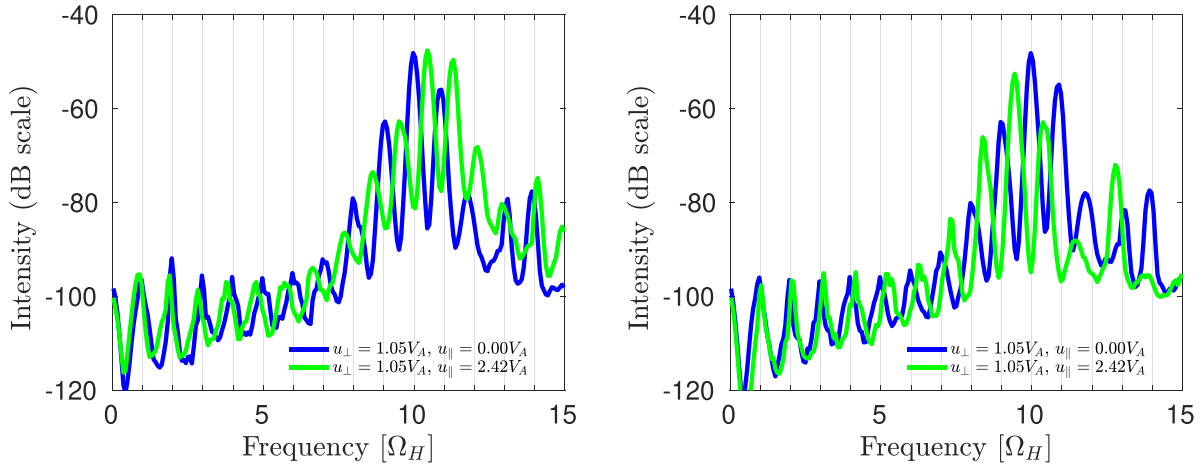


Figure 22. Power spectra of δB_z from PIC-hybrid computations with the orientation of the spatial domain $\hat{\mathbf{x}}$ at an angle of 91.0° with respect to the background magnetic field. Excited waves propagating in both the $+\hat{\mathbf{x}}$ direction (left panel) and in the $-\hat{\mathbf{x}}$ direction (right panel) are included. The initial energetic proton distribution functions are $[n_H/(2\pi v_\perp)]\delta(v_\parallel)\delta(v_\perp - u_\perp)$ (blue trace) and $[n_H/(2\pi u_\perp)]\delta(v_\parallel - u_\parallel)\delta(v_\perp - u_\perp)$ (green trace). The velocities are $u_\parallel = 2.199 \times 10^7 \text{ ms}^{-1}$ and $u_\perp = 0.956 \times 10^7 \text{ ms}^{-1}$, corresponding to $u_\perp = 1.05V_A$ and $u_\parallel = 2.42V_A$ and are such that $m_H(u_\parallel^2 + u_\perp^2)/2 = 3.02 \text{ MeV}$. The dominant spectral peaks for the green traces are at: (left) $9.50\Omega_H$, $10.44\Omega_H$ and $11.30\Omega_H$; (right) $8.37\Omega_H$, $9.44\Omega_H$ and $10.37\Omega_H$.

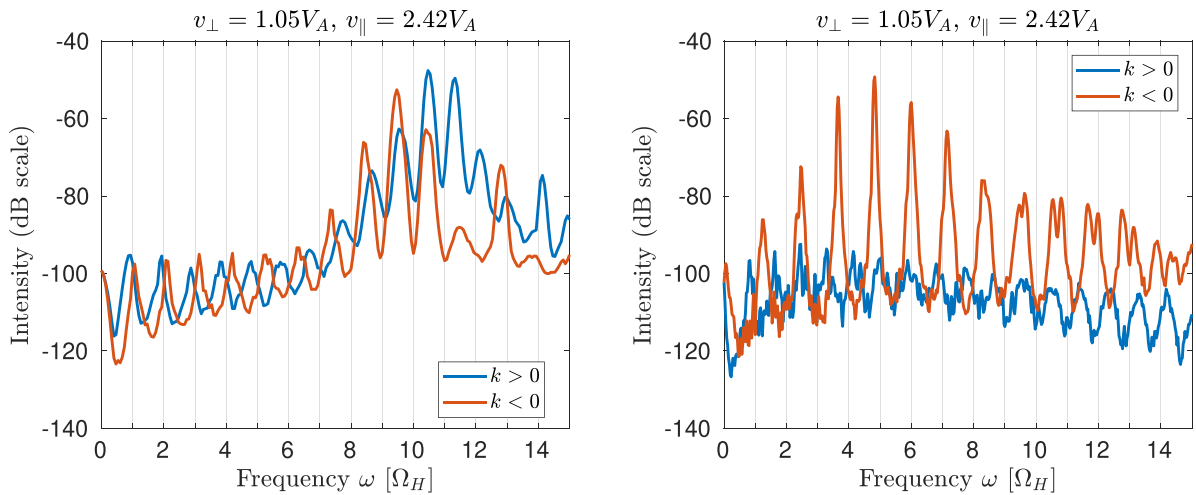


Figure 23. Power spectra obtained at a propagation angle of 89° (left) and 85° (right). The simulation parameters are given in the text.

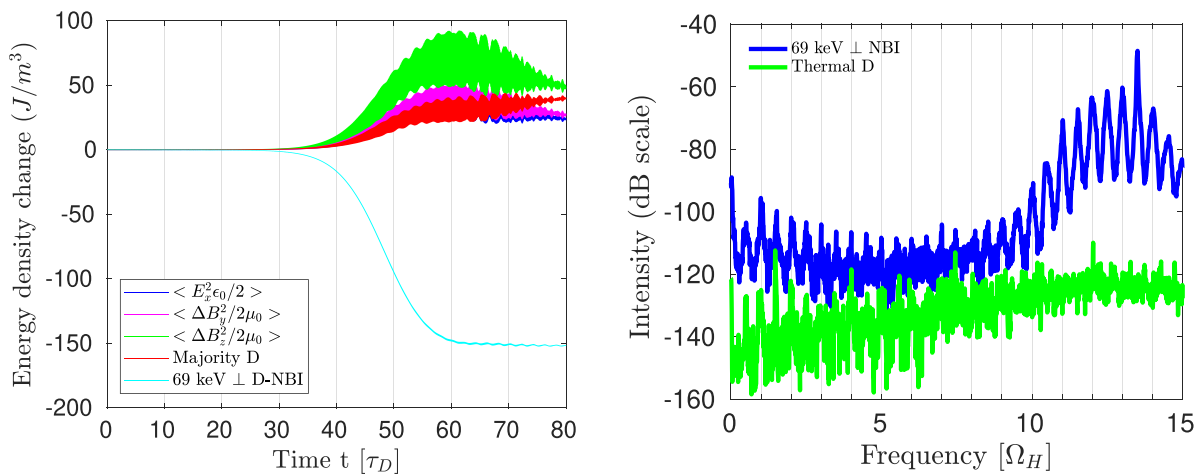


Figure 24. Time evolution of the change in energy density of the electric and magnetic fields and of the ion species following the relaxation of a 69 keV deuteron NBI population (left). Power spectrum of the fluctuating δB_z averaged over the simulation duration together with the thermal noise of the thermal deuteron plasma.

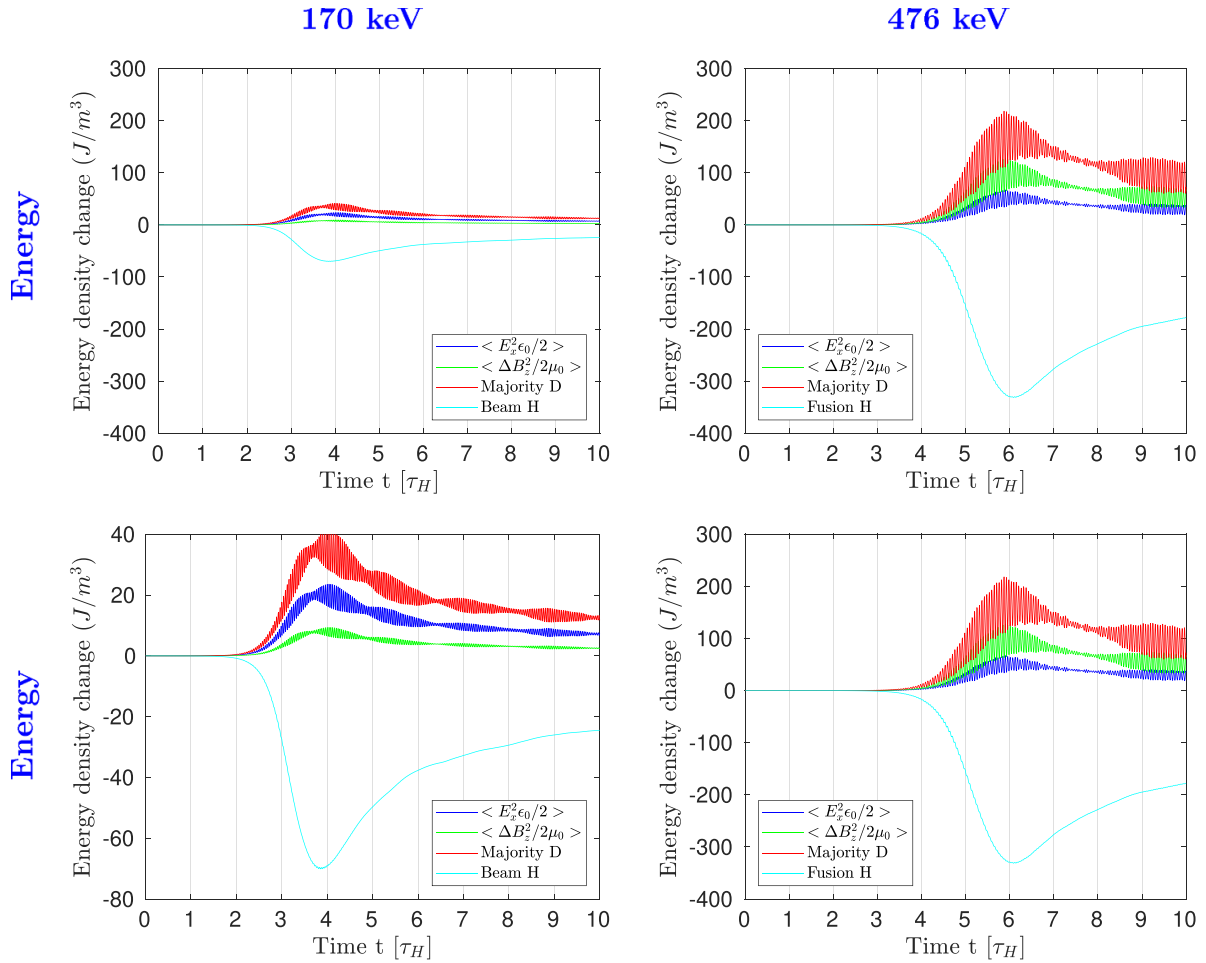


Figure 25. Energy density time evolution of fields and thermal deuterons together with energetic minority proton population initialised as a ring-beam $n_H/(2\pi v_\perp)\delta(v_\parallel)\delta(v_\perp - u_\perp)$ in a full-PIC simulation. The electron density is $n_e = 8.8 \times 10^{18} \text{ m}^{-3}$ and the background magnetic field is $B_0 = 1.75 \text{ T}$, perpendicular to the simulation domain. The electron and deuterium temperatures are respectively 846 eV and 907 eV. These correspond to the parameters during the transient ICE event in LHD plasma 133979. Left and right panels correspond respectively to 170 keV beam protons and 476 keV fusion-born protons characterised by $u_\perp/V_A = 0.627$ and $u_\perp/V_A = 1.050$. Since the propagation angle is exactly 90° , no spectral shifts would be observed if a non-zero parallel velocity component was included. This motivates the relaxation of two different energetic proton population of which energy is solely in the perpendicular velocity component. In addition, the lower hybrid frequency is minimal at 90° and leads to the lowest harmonics that these proton population can excite when the electron density is $8.8 \times 10^{18} \text{ m}^{-3}$. The top panels share the same energy scales and show that the fusion-born proton population with $E_\perp = 476 \text{ keV}$ releases $5\times$ more energy than the 170 keV proton beam at equal relative density $\xi = n_H/n_e = 0.002$. The second qualitative difference comes from the nature of the fields excited: predominantly electrostatic with 170 keV protons and electromagnetic with 476 keV protons. The top left energy time evolution panel is zoomed on the bottom left panel and the panel on the top right is reproduced at the bottom right.

a different (higher) range of frequencies. It also shows that both even and odd deuteron cyclotron harmonics are excited and preferentially at higher frequencies compared to those of the present work. The fusion-born protons are able to drive strongly and simultaneously ICE at cyclotron harmonics 8th–12th while the calculation with 69 keV NBI deuterons suggests strong excitations above $11\Omega_H$. The inclusion of a parallel velocity component would further decrease the energy in the perpendicular component and thus lower the drive of ICE. Simulations of NBI deuterons in LHD deuterium plasma have also been presented in [62]. We have also focused on the disentanglement of ICE driven by fusion-born protons and 170 keV parallel-NBI protons. We have performed fully kinetic simulations that compare the drive of energetic

protons initialised in velocity space with a ring-beam distribution $\propto \delta(v_\perp - u_\perp)$ where the value u_\perp is chosen to correspond either to a 170 keV NBI proton population or a 476 keV Alfvénic subpopulation of fusion-born protons in LHD. We have initialised our full-PIC calculations using 1400 macroparticles per cell and per species (electrons, thermal deuterons and energetic protons) on a one-dimensional simulation domain consisting of 50 000 cells of size $0.9\lambda_{De}$, with the electron Debye length $\lambda_{De} = 7.29 \times 10^{-5} \text{ m}$. The relative energetic proton population is $\xi = 0.002$ and the angle between the background magnetic field and the simulation domain is 90° . The thermal electron temperature and density together with the thermal deuteron temperature are identical to those of the relaxation calculation of the 69 keV NBI deuterons. The

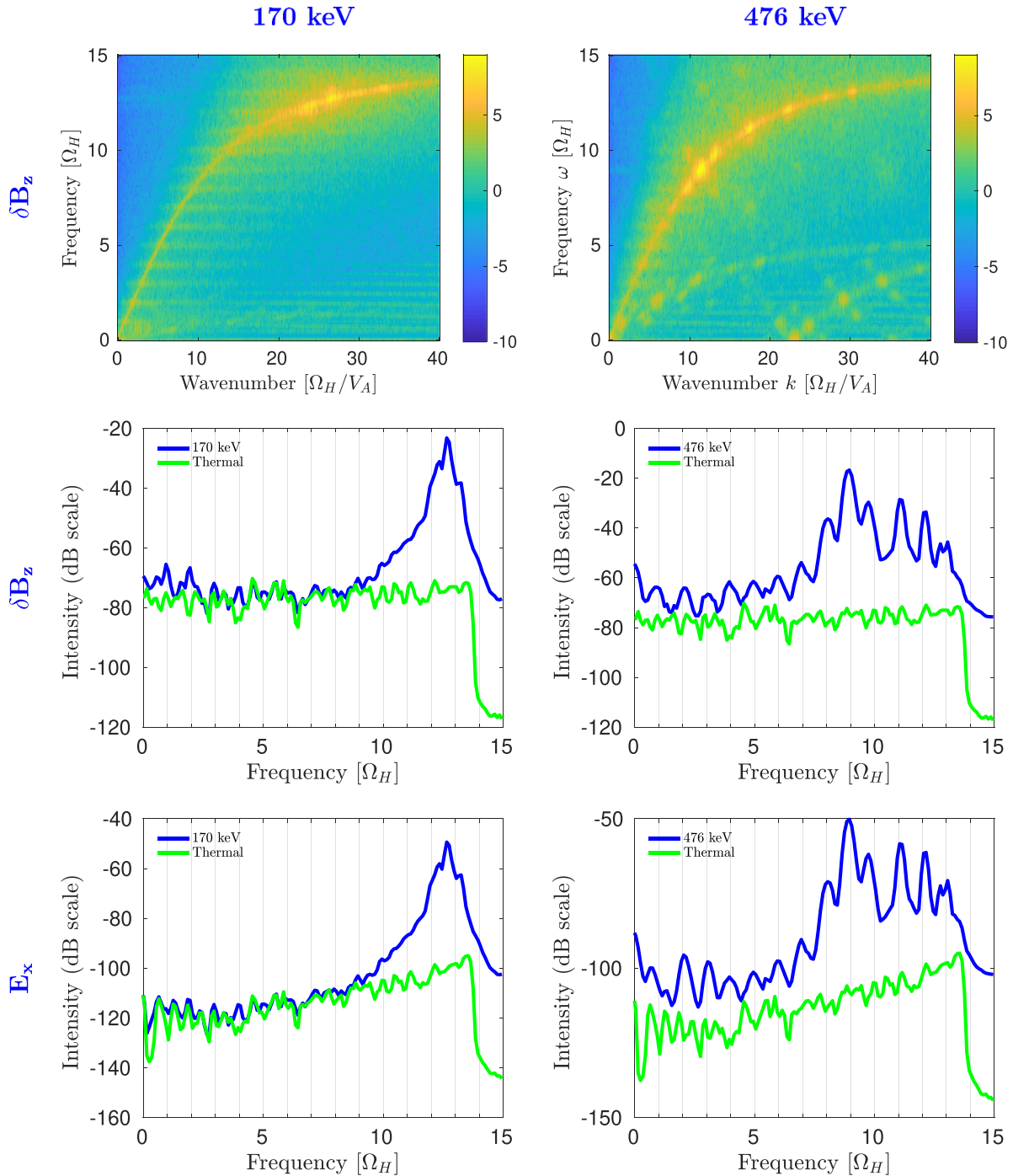


Figure 26. Spectral power on a \log_{10} scale resulting from the spatiotemporal fast Fourier transform of the z -component of the perturbed magnetic field (top) taken over the simulation duration (10 proton gyroperiods) and over the entire simulation domain ($50\,000\lambda_{De}$). The left panels relate to the relaxation of a 170 keV proton beam and the right panels to a proton population of 476 keV. In both cases, these energetic proton populations are initialised as ring-beams $n_H/(2\pi v_\perp)\delta(v_\parallel)\delta(v_\perp - u_\perp)$ such that the energy is concentrated in the perpendicular velocity components and the parallel energies are initialised to zero. Averaging the dispersion relation on the top panels between $k=0$ and $k=40\Omega_H/V_A$ gives rise to the power spectra on the middle panels represented on a dB scale as shown by the blue curves. The green curves represent the noise level obtained by running a simulation with thermal electrons and deuterons only. A similar procedure is conducted for the x -component of the electric-field and leads to the bottom panels. The spectral character differs in that excitations evolve from predominantly electrostatic excitation with the relaxation of 170 keV protons to mainly electromagnetic excitations with 476 keV protons. These populations have no parallel velocity component. The 170 keV sub-Alfvénic proton population ($u_\perp/V_A = 0.672$) gives rise to one major peak, whose maximum is not necessarily at an integer cyclotron harmonic, and locates between $12\Omega_H$ and $13\Omega_H$. Increasing the energy leads to the Alfvénic regime of the 476 keV energetic protons ($u_\perp/V_A = 1.050$) displaying excitations of the MCI between $8\Omega_H$ and $12\Omega_H$ which we shall refer to as the MCI sector.

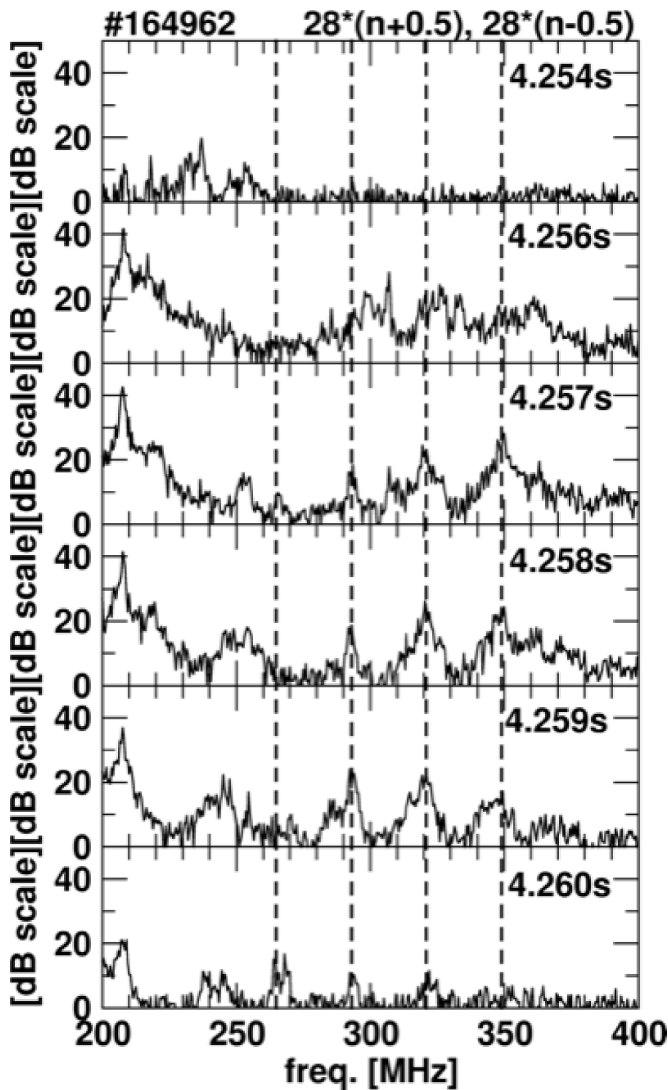


Figure 27. Measured power spectrum detected by the dipole antenna in LHD plasma 164962 at $t = 4.255$ s. The most intense spectral peaks have frequencies which correspond to $28 \times (n + 0.5)$ MHz and $28 \times (n - 0.5)$ MHz, where n is an integer, and are therefore identified as highly shifted cyclotron harmonics of the energetic protons.

simulation results in figures 25 and 26 suggest that the frequencies that are most strongly driven by 170 keV NBI protons locate around the 12th proton cyclotron harmonic while the LHD measured power spectra of figure 2 indicate excitations in the range 8th–11th cyclotron harmonics.

Appendix D. Frequency shifts not unique to LHD plasma 133979

In LHD plasma 164962, for which $R_{ax} = 3.6$ m and $B_t = 2.85$ T, bursting ICE was observed with spectral peaks corresponding to large frequency shifts with respect to cyclotron harmonics identified with the fusion-born protons. Figure 27 shows that these peaks correspond to either $28 \times (n + 0.5)$ MHz or $28 \times (n - 0.5)$ MHz.

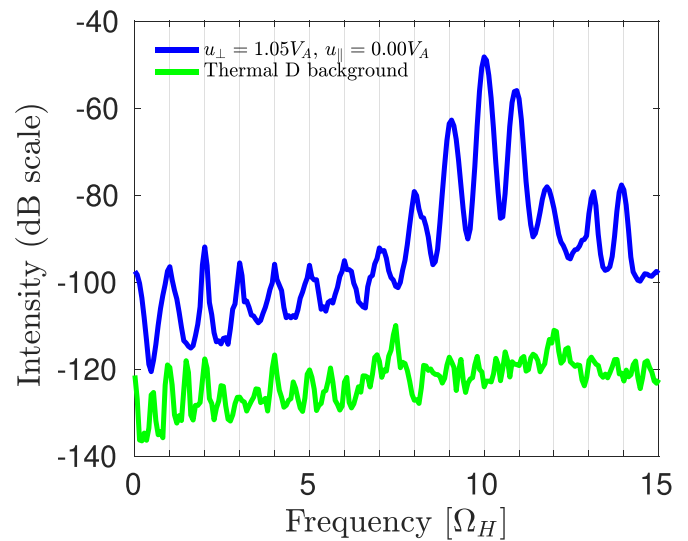


Figure 28. Simulated power spectra obtained for the simulation parameters given in section 4.3, namely 2000 macroparticles per cell and per ion species and 8192 cells, $\xi = 0.001$ and 91° propagation angle. The green trace corresponds to the spectrum obtained without energetic protons.

Appendix E. Noise in the simulation

We have quantified the noise level in our hybrid PIC calculations by running one simulation which consists of a deuterium thermal plasma only. We do not compare it with the noise arising from the LHD detection system. Our purpose is only to show that a good signal-to-noise ratio is achieved in our calculations. The thermal plasma shows preferential excitations at normal modes, which are the cyclotron harmonics as per the green trace in figure 28 in agreement with the fluctuation dissipation theorem [79].

ORCID iDs

B C G Reman <https://orcid.org/0000-0003-3507-9444>
 H Igami <https://orcid.org/0000-0002-4541-1757>
 S C Chapman <https://orcid.org/0000-0003-0053-1584>
 S Inagaki <https://orcid.org/0000-0002-4808-857X>
 M H Kim <https://orcid.org/0000-0002-7481-4600>
 G S Yun <https://orcid.org/0000-0002-1880-5865>

References

- [1] Takeiri Y *et al* 2017 Extension of the operational regime of the LHD towards a deuterium experiment *Nucl. Fusion* **57** 102023
- [2] Osakabe M *et al* 2017 Current status of large helical device and its prospect for deuterium experiment *Fusion Sci. Technol.* **72** 199–210
- [3] Takeiri Y 2018 The large helical device: entering deuterium experiment phase toward steady-state helical fusion reactor based on achievements in hydrogen experiment phase *IEEE Trans. Plasma Sci.* **46** 2348–53
- [4] Osakabe M, Isobe M, Tanaka M, Motojima G, Tsumori K, Yokoyama M, Morisaki T and Takeiri Y 2018 Preparation

- and commissioning for the LHD deuterium experiment *IEEE Trans. Plasma Sci.* **46** 2324–31
- [5] Kobayashi M *et al* 2018 First measurements of thermal neutron distribution in the LHD torus hall generated by deuterium experiments *Fusion Eng. Des.* **137** 191–5
- [6] Isobe M *et al* 2018 Fusion neutron production with deuterium neutral beam injection and enhancement of energetic-particle physics study in the large helical device *Nucl. Fusion* **58** 082004
- [7] Tanaka T, Yoshihashi S, Kobayashi M, Uritani A, Watanabe K, Yamazaki A, Nishitani T, Ogawa K and Isobe M 2019 Measurement of neutron spectrum using activation method in deuterium plasma experiment at LHD *Fusion Eng. Des.* **146** 496–9
- [8] Muscatello C, Heidbrink W, Boivin R, Chrystal C, Collins C, Fujiwara Y and Yamaguchi H 2019 Diagnosis of fast ions produced by negative-ion neutral-beam injection with fast-ion deuterium-alpha spectroscopy *Rev. Sci. Instrum.* **90** 073504
- [9] Cottrell G and Dendy R 1988 Superthermal radiation from fusion products in JET *Phys. Rev. Lett.* **60** 33
- [10] Cottrell G, Bhatnagar V, Da Costa O, Dendy R, Jacquinet J, McClements K, McCune D, Nave M, Smeulders P and Start D 1993 Ion cyclotron emission measurements during JET deuterium-tritium experiments *Nucl. Fusion* **33** 1365
- [11] Saito K *et al* 2009 Measurement of ion cyclotron emissions by use of ICRF heating antennas in LHD *Fusion Eng. Des.* **84** 1676–9
- [12] Saito K *et al* 2013 Measurement of ion cyclotron emissions by using high frequency magnetic probes in the LHD *Plasma Sci. Technol.* **15** 209
- [13] Saito K *et al* 2018 Rf wave detection with high-frequency magnetic probes in LHD *Plasma Fusion Res.* **13** 3402043
- [14] Reman B, Dendy R, Akiyama T, Chapman S, Cook J, Igami H, Inagaki S, Saito K and Yun G 2019 Interpreting observations of ion cyclotron emission from large helical device plasmas with beam-injected ion populations *Nucl. Fusion* **59** 096013
- [15] Reman B *et al* 2021 Density dependence of ion cyclotron emission from deuterium plasmas in the large helical device *Nucl. Fusion* **61** 066023
- [16] Du X *et al* 2015 Resistive interchange modes destabilized by helically trapped energetic ions in a helical plasma *Phys. Rev. Lett.* **114** 155003
- [17] Du X *et al* 2015 Resistive interchange mode destabilized by helically trapped energetic ions and its effects on energetic ions and bulk plasma in a helical plasma *Nucl. Fusion* **56** 016002
- [18] Michael C *et al* 2018 Role of helium–hydrogen ratio on energetic interchange mode behaviour and its effect on ion temperature and micro-turbulence in LHD *Nucl. Fusion* **58** 046013
- [19] Ohdachi S, Bando T, Nagaoka K, Takahashi H, Suzuki Y, Watanabe K, Du X, Toi K, Osakabe M and Morisaki T 2018 Excitation mechanism of the energetic particle driven resistive interchange mode and strategy to control the mode in large helical device *27th IAEA Fusion Energy Conf. (Gandhinagar, India)* pp 22–27 (available at: <https://nucleus.iaea.org/sites/fusionportal/Shared%20Documents/FEC%202018/fec2018-preprints/preprint0128.pdf>)
- [20] Bando T *et al* 2018 Excitation of helically-trapped-energetic-ion driven resistive interchange modes with intense deuterium beam injection and enhanced effect on beam ions/bulk plasmas of LHD *Nucl. Fusion* **58** 082025
- [21] Ida K, Kobayashi T, Itoh K, Yoshinuma M, Tokuzawa T, Akiyama T, Moon C, Tsuchiya H, Inagaki S and Itoh S-I 2016 Abrupt onset of tongue deformation and phase space response of ions in magnetically-confined plasmas *Sci. Rep.* **6** 36217
- [22] Ida K, Kobayashi T, Yoshinuma M, Akiyama T, Tokuzawa T, Tsuchiya H, Itoh K and Group L E 2017 Observation of distorted Maxwell-Boltzmann distribution of epithermal ions in LHD *Phys. Plasmas* **24** 122502
- [23] Ida K, Kobayashi T, Yoshinuma M, Akiyama T, Tokuzawa T, Tsuchiya H, Itoh K and Itoh S-I 2018 Trigger mechanism for the abrupt loss of energetic ions in magnetically confined plasmas *Sci. Rep.* **8** 2804
- [24] Thatipamula S G, Yun G, Leem J, Park H K, Kim K, Akiyama T and Lee S 2016 Dynamic spectra of radio frequency bursts associated with edge-localized modes *Plasma Phys. Control. Fusion* **58** 065003
- [25] Kim M, Thatipamula S G, Lee J, Choi M J, Park H K, Akiyama T and Yun G S 2018 Distinct stages of radio frequency emission at the onset of pedestal collapse in KSTAR H-mode plasmas *Nucl. Fusion* **58** 096034
- [26] Kim M, Thatipamula S G, Kim J, Choi M J, Lee J, Lee W, Kim M, Yoon Y and Yun G S 2020 Intense whistler-frequency emissions at the pedestal collapse in KSTAR H-mode plasmas *Nucl. Fusion* **60** 126021
- [27] Chapman B, Dendy R, McClements K, Chapman S, Yun G, Thatipamula S and Kim M 2017 Sub-microsecond temporal evolution of edge density during edge localized modes in KSTAR tokamak plasmas inferred from ion cyclotron emission *Nucl. Fusion* **57** 124004
- [28] Chapman B, Dendy R O, Chapman S C, McClements K G, Yun G S, Thatipamula S G and Kim M 2018 Nonlinear wave interactions generate high-harmonic cyclotron emission from fusion-born protons during a KSTAR ELM crash *Nucl. Fusion* **58** 096027
- [29] Ichimura M *et al* 2008 Study of ion cyclotron emissions due to DD fusion product ions on JT-60U EX/P8-2 *22nd IAEA Fusion Energy Conf. (Geneva)* (available at: https://www-pub.iaea.org/MTCD/Meetings/FEC2008/ex_p8-2.pdf)
- [30] Sato S *et al* 2010 Observation of ion cyclotron emission owing to DD fusion product H ions in JT-60U *Plasma Fusion Res.* **5** S2067
- [31] Ichimura M, Higaki H, Kakimoto S, Yamaguchi Y, Nemoto K, Katano M, Ishikawa M, Moriyama S and Suzuki T 2008 Observation of spontaneously excited waves in the ion cyclotron frequency range on JT-60U *Nucl. Fusion* **48** 035012
- [32] Winske D and Omidi N 1991 Hybrid codes: methods and applications *4th Int. School for Space Simulation (Nara, Japan 1–5 Apr 1991)* pp 1–5 (available at: <https://ui.adsabs.harvard.edu/abs/1991issr.reptR...1W/abstract>)
- [33] Winske D, Yin L, Omidi N, Karimabadi H and Quest K 2003 Hybrid simulation codes: past, present and future—a tutorial *Space Plasma Simulation* (Berlin: Springer) pp 136–65 (available at: https://link.springer.com/chapter/10.1007/3-540-36530-3_8)
- [34] Carbajal L, Dendy R O, Chapman S and Cook J 2014 Linear and nonlinear physics of the magnetoacoustic cyclotron instability of fusion born-ions in relation to ion cyclotron emission *Phys. Plasmas* **21** 012106
- [35] Carbajal L, Dendy R, Chapman S and Cook J 2017 Quantifying fusion born ion populations in magnetically confined plasmas using ion cyclotron emission *Phys. Rev. Lett.* **118** 105001
- [36] Chapman B, Dendy R, Chapman S, McClements K, Yun G, Thatipamula S and Kim M 2019 Interpretation of suprathermal emission at deuteron cyclotron harmonics from deuterium plasmas heated by neutral beam injection in the KSTAR tokamak *Nucl. Fusion* **59** 106021
- [37] Ochoukov R *et al* 2018 Core plasma ion cyclotron emission driven by fusion-born ions *Nucl. Fusion* **59** 014001

- [38] Ochoukov R *et al* 2018 Observations of core ion cyclotron emission on ASDEX Upgrade tokamak *Rev. Sci. Instrum.* **89** 10J101
- [39] Ochoukov R *et al* 2019 Interpretation of core ion cyclotron emission driven by sub-Alfvénic beam-injected ions via magnetoacoustic cyclotron instability *Nucl. Fusion* **59** 086032
- [40] Chapman B, Dendy R, Chapman S, McClements K and Ochoukov R 2020 Origin of ion cyclotron emission at the proton cyclotron frequency from the core of deuterium plasmas in the ASDEX-Upgrade tokamak *Plasma Phys. Control. Fusion* **62** 095022
- [41] Cauffman S and Majeski R 1995 Ion cyclotron emission on the Tokamak Fusion Test Reactor *Rev. Sci. Instrum.* **66** 817–9
- [42] Cook J, Dendy R O and Chapman S 2013 Particle-in-cell simulations of the magnetoacoustic cyclotron instability of fusion-born alpha particles in tokamak plasmas *Plasma Phys. Control. Fusion* **55** 065003
- [43] Cook J, Dendy R and Chapman S 2017 Stimulated emission of fast Alfvén waves within magnetically confined fusion plasmas *Phys. Rev. Lett.* **118** 185001
- [44] Chapman B, Dendy R, Chapman S, Holland L, Irvine S and Reman B 2020 Comparing theory and simulation of ion cyclotron emission from energetic ion populations with spherical shell and ring-beam distributions in velocity-space *Plasma Phys. Control. Fusion* **62** 055003
- [45] Belikov V and Kolesnichenko I I 1976 Magnetoacoustic cyclotron instability in a thermonuclear plasma *Sov. Phys. Tech. Phys.* **20** 1146–51
- [46] Dendy R, Lashmore Davies C N and Kam K 1992 A possible excitation mechanism for observed superthermal ion cyclotron emission from tokamak plasmas *Phys. Fluids B* **4** 3996–4006
- [47] McClements K and Dendy R 1993 Ion cyclotron harmonic wave generation by ring protons in space plasmas *J. Geophys. Res.: Space Phys.* **98** 11689–700
- [48] Dendy R and McClements K 1993 Ion cyclotron wave emission at the quasi-perpendicular bow shock *J. Geophys. Res.: Space Phys.* **98** 15531–9
- [49] Dendy R O, Lashmore Davies C and Kam K F 1993 The magnetoacoustic cyclotron instability of an extended shell distribution of energetic ions *Phys. Fluids B* **5** 1937–44
- [50] Dendy R, Lashmore-Davies C, McClements K and Cottrell G 1994 The excitation of obliquely propagating fast Alfvén waves at fusion ion cyclotron harmonics *Phys. Plasmas* **1** 1918–28
- [51] Dendy R, McClements K, Lashmore-Davies C, Majeski R and Cauffman S 1994 A mechanism for beam-driven excitation of ion cyclotron harmonic waves in the Tokamak Fusion Test Reactor *Phys. Plasmas* **1** 3407–13
- [52] Cauffman S, Majeski R, McClements K and Dendy R 1995 Alfvénic behaviour of alpha particle driven ion cyclotron emission in TFTR *Nucl. Fusion* **35** 1597
- [53] Dendy R, McClements K, Lashmore Davies C, Cottrell G, Majeski R and Cauffman S 1995 Ion cyclotron emission due to collective instability of fusion products and beam ions in TFTR and JET *Nucl. Fusion* **35** 1733
- [54] McClements K G, Dendy R, Lashmore Davies C, Cottrell G, Cauffman S and Majeski R 1996 Interpretation of ion cyclotron emission from sub-Alfvénic fusion products in the Tokamak Fusion Test Reactor *Phys. Plasmas* **3** 543–53
- [55] Matsumoto Y, Nagaura T, Oikawa S-I and Watanabe T 2004 Particle orbit analysis under the ion cyclotron range of frequency heating in the large helical device *Jpn. J. Appl. Phys.* **43** 332
- [56] Seki R, Matsumoto Y, Suzuki Y, Watanabe K and Itagaki M 2008 Particle orbit analysis in the finite beta plasma of the large helical device using real coordinates *Plasma Fusion Res.* **3** 016
- [57] McClements K, Hunt C, Dendy R and Cottrell G 1999 Ion cyclotron emission from JET DT plasmas *Phys. Rev. Lett.* **82** 2099–102
- [58] McClements K G, Brisset A, Chapman B, Chapman S C, Dendy R O, Jacquet P, Kiptily V, Mantsinen M and Reman B C (JET Contributors) 2018 Observations and modelling of ion cyclotron emission observed in jet plasmas using a sub-harmonic arc detection system during ion cyclotron resonance heating *Nucl. Fusion* **58** 096020
- [59] Moseev D and Salewski M 2019 Bi-Maxwellian, slowing-down and ring velocity distributions of fast ions in magnetized plasmas *Phys. Plasmas* **26** 020901
- [60] Dendy R and McClements K 2015 Ion cyclotron emission from fusion-born ions in large tokamak plasmas: a brief review from JET and TFTR to ITER *Plasma Phys. Control. Fusion* **57** 044002
- [61] Liu L *et al* 2021 Explanation of core ion cyclotron emission from beam-ion heated plasmas in ASDEX Upgrade by the magnetoacoustic cyclotron instability *Nucl. Fusion* **61** 026004
- [62] Toida M, Igami H, Saito K, Akiyama T, Kamio S and Seki R 2019 Simulation study of energetic ion driven instabilities near the lower hybrid resonance frequency in a plasma with increasing density *Plasma Fusion Res.* **14** 3401112
- [63] Thome K, Pace D, Pinsker R, Meneghini O, del Castillo C and Zhu Y 2018 Radio frequency measurements of energetic-particle-driven emission using the ion cyclotron emission diagnostic on the DIII-D tokamak *Rev. Sci. Instrum.* **89** 10I102
- [64] Thome K E, Pace D C, Pinsker R I, Van Zeeland M A, Heidbrink W W and Austin M E 2019 Central ion cyclotron emission in the DIII-D tokamak *Nucl. Fusion* **59** 086011
- [65] DeGrandchamp G, Thome K, Heidbrink W, Holmes I and Pinsker R 2021 Upgrades to the ion cyclotron emission diagnostic on the DIII-D tokamak *Rev. Sci. Instrum.* **92** 033543
- [66] Salewski M *et al* 2014 Measurement of a 2D fast-ion velocity distribution function by tomographic inversion of fast-ion D-alpha spectra *Nucl. Fusion* **54** 023005
- [67] Moseev D, Salewski M, Garcia-Muñoz M, Geiger B and Nocente M 2018 Recent progress in fast-ion diagnostics for magnetically confined plasmas *Rev. Mod. Plasma Phys.* **2** 7
- [68] Salewski M *et al* 2019 Diagnostic of fast-ion energy spectra and densities in magnetized plasmas *J. Instrum.* **14** C05019
- [69] Moseev D *et al* 2021 Development of the ion cyclotron emission diagnostic for the w7-x stellarator *Rev. Sci. Instrum.* **92** 033546
- [70] Schmidt B, Salewski M, Reman B, Dendy R, Moseev D, Ochoukov R, Fasoli A, Baquero-Ruiz M and Järleblad H 2021 Determining 1D fast-ion velocity distribution functions from ion cyclotron emission data using deep neural networks *Rev. Sci. Instrum.* **92** 053528
- [71] McClements K, D'Inca R, Dendy R, Carbajal L, Chapman S, Cook J, Harvey R, Heidbrink W and Pinches S 2015 Fast particle-driven ion cyclotron emission (ICE) in tokamak plasmas and the case for an ICE diagnostic in ITER *Nucl. Fusion* **55** 043013
- [72] Yun G and Akiyama T 2012 Fast RF spectrometer system on LHD *Annual Report of National Institute for Fusion Science* p 46 (available at: <http://hdl.handle.net/10655/10804>)
- [73] Yun G and Akiyama T 2013 Fast RF spectrometer system on LHD *Annual Report of National Institute for Fusion Science* p 53 (available at: <http://hdl.handle.net/10655/11673>)

- [74] Yun G and Akiyama T 2014 Fast RF spectrometer system on LHD *Annual Report of National Institute for Fusion Science* p 58
- [75] Fredrickson E D, Gorelenkov N, Bell R, Diallo A, LeBlanc B, Podestà M and Team N 2019 Emission in the ion cyclotron range of frequencies (ICE) on NSTX and NSTX-U *Phys. Plasmas* **26** 032111
- [76] Mutoh T *et al* 2007 Steady-state operation and high energy particle production of mev energy in the large helical device *Nucl. Fusion* **47** 1250
- [77] Watanabe T, Miyazawa J, Yamada H, Murakami S, Masuzaki S, Osakabe M, Isobe M, Tokitani M and Motojima O 2008 Discriminating acquisition of 15-meV protons from D-3He fusion reaction in LHD *Plasma Fusion Res.* **3** 058
- [78] Fülöp T and Lisak M 1998 Ion cyclotron emission from fusion products and beam ions in the Tokamak Fusion Test Reactor *Nucl. Fusion* **38** 761
- [79] Kubo R 1966 The fluctuation-dissipation theorem *Rep. Prog. Phys.* **29** 255